



TRABALHO DE CONCLUSÃO DE CURSO

**POWER DISTRIBUTION SYSTEM:
LOAD MODELING OF A POWER DISTRIBUTION
SYSTEM (PDS) FOR A MEDICAL IMAGING
PROCESSOR**

Por,

Marina Gasparini de Barros

Vesna Resende Barros

Brasília, Dezembro de 2013

UNIVERSIDADE DE BRASÍLIA
Faculdade de Tecnologia
Curso de Graduação em Engenharia Elétrica

TRABALHO DE CONCLUSÃO DE CURSO

**POWER DISTRIBUTION SYSTEM:
LOAD MODELING OF A POWER DISTRIBUTION
SYSTEM (PDS) FOR A MEDICAL IMAGING
PROCESSOR**

POR,

Marina Gasparini de Barros

Vesna Resende Barros

Relatório submetido como requisito parcial para obtenção
do grau de Engenheiro Eletricista.

Banca Examinadora

Prof. Anésio de Leles Ferreira Filho, UnB/ ENE
(Orientador)

Prof. Pablo Eduarco Cuervo Franco, UnB/ENE

Prof. Jorge Cormane, UnB/ENE

Brasília, Dezembro de 2013

FICHA CATALOGRÁFICA

GASPARINI DE BARROS, MARINA; RESENDE BARROS, VESNA

Power distribution system: Load modeling of a power distribution system (PDS) for a medical imaging processor [Distrito Federal] 2013

xi, 60p., 297 mm (FT/UnB, Engenheiro, Eletricista, 2014). Trabalho de Graduação – Universidade de Brasília. Faculdade de Tecnologia.

1. Power Distribution System

2. Load Modeling

3. LTspice

I. Elétrica/FT/UnB

REFERÊNCIA BIBLIOGRÁFICA

BARROS, VR; GASPARINI, M (2013). Power distribution system: Load modeling of a power distribution system (PDS) for a medical imaging processor. Trabalho de Graduação em Engenharia Elétrica, Faculdade de Tecnologia, Universidade de Brasília, Brasília, DF, 60p.

CESSÃO DE DIREITOS

AUTOR: Marina Gasparini de Barros e Vesna Resende Barros.

POWER DISTRIBUTION SYSTEM: Load modeling of a power distribution system (PDS) for a medical imaging processor.

GRAU: Engenheiro

ANO: 2014

É concedida à Universidade de Brasília permissão para reproduzir cópias deste Trabalho de Graduação e para emprestar ou vender tais cópias somente para propósitos acadêmicos e científicos. O autor reserva outros direitos de publicação e nenhuma parte desse Trabalho de Graduação pode ser reproduzida sem autorização por escrito do autor.

Marina Gasparini de Barros
SMAS Trecho 01 Lote C
Bloco C Ap. 616 – Living Park Sul
71218-010 Guará – DF – Brasil

Vesna Resende Barros
SQN 212 Bloco H Ap. 401 – Asa Norte
70864-080 Brasília – DF – Brasil

AGRADECIMENTOS

Dedico esta obra aos meus pais, Fátima e Paulo, por todo o suporte, amor e incentivo ao longo de todos esses anos. Sem o grande esforço de ambos, provavelmente não haveria chegado até aqui.

Ao meu grande companheiro e amor, Gilberto, pelo seu carinho, companheirismo e dedicação sempre presentes, principalmente durante os meses que passamos longe para que este trabalho de fim de curso fosse concretizado.

À minha amiga e companheira, Vesna, por todo apoio e dedicação para a realização deste trabalho.

Obrigada a todos. Amo vocês.

Marina Gasparini.

Aos meus amados pais, Sirleny e Lucas, por todo carinho, amor, dedicação e apoio doados a mim em cada passo da minha vida.

Aos eternos amigos, Cecília, Danielli, Marcelo e Vanessa, por darem significado as palavras companheirismo, cumplicidade e lealdade.

À minha companheira de projeto, Marina, pela grande amizade e por estar presente ao meu lado durante essa caminhada.

A todos os colegas de curso.

Vesna Resende Barros

ABSTRACT

Philips Healthcare is researching and developing a new power distribution architecture that is intended to power different medical equipment, such as computed tomography, radiography, ultrasound and interventional X-ray equipment. The objective of this new architecture is to improve the safety in using these medical devices during operations, but it is further intended to power other non-medical devices as well.

Some parts of the new architecture, like the power source and the Power Distribution System (PDS) have already been designed by Philips and former students. However, the load model that is connected to the system still needs to be tested and validated in order to have the whole architecture completed.

Therefore, this report contains the results obtained after six months studying the loads characteristics of the system. A computational model was designed in LTspice IV software to predict the behavior of different loads when connected to the PDS. In the model, the load was represented by electronic components described by values that change over time. These values are set by the user with the purpose of analyzing the variations of voltage and currents during the load operation time, and they were carefully chosen in order to provide the results most similar to real life.

After simulating, measurements with real loads in the X-Ray laboratory were analyzed and compared with the previous computational results. A validation tool was used to verify the closeness of the simulations to the practical measurements. In preparing and designing the models, an accuracy of 10% between the models and the practical results is expected.

Keywords: Power Distribution System; Load Modeling; LTspice

CONTENTS

Assignment Description.....	12
1. Introduction.....	15
1.1 Electric Power Distribution System	16
1.2 Inrush Current.....	17
2. Magnetic Components.....	20
3. Load Model Building.....	26
1.3 Software Simulation.....	26
1.4 Data Interpolation	32
4. Practical Analysis	35
5. Results and Discussion.....	43
6. Conclusions	46
Appendix A – Load Modeling.....	48
Appendix B – Load Types	51
Appendix C – Computational Model.....	57
Appendix D – Lab Measurements.....	63
References	73

LIST OF FIGURES

Figure 1: Power Flow Diagram.....	12
Figure 2: Power Distribution System Schematic.....	14
Figure 3: Overview of Electrical Distribution System	16
Figure 4: Three phase AC waveform	17
Figure 5: Current waveform when the device is powered up	18
Figure 6: The electric circuit of an ideal transformer.....	20
Figure 7: Equivalent electric circuit of saturable core model.....	21
Figure 8: Complete transformer model.....	22
Figure 9: The result when simulating the complete transformer model.....	23
Figure 10: Results obtained when the amplitude of the input voltage source was varied and set as (a) 2 volts, (b) 5 volts and (c) 10 volts.....	24
Figure 11: Hysteresis curve and output voltages and current obtained with the source switched on at (a) 0° and (b) 90°	25
Figure 12: Single phase load described as a mathematical function	27
Figure 13: Voltage at the source and current at the load.....	28
Figure 14: DCPS VWCB receiver modules (B-Cabinet)	28
Figure 15: DCPS VWCB receiver modules (B-Cabinet)	28
Figure 16: CRCB continuous (M-Cabinet).....	29
Figure 17: SIB (M-cabinet).....	29
Figure 18: Host PC (M-Cabinet).....	29
Figure 19: Tube Cooler F (M-Cabinet)	30
Figure 20: Circuit model (CRCB monitor).....	31
Figure 21: Simulation of CRCB monitor circuit model.....	31
Figure 22: Linear interpolation between two points.	32
Figure 23: Validation CRCB monitor model.....	33
Figure 24: Monitor's waveforms when the power is switched on at 0° (on the left) and at 90° (on the right)	35

Figure 25: DCPS's waveforms when the power is switched on at 0° (on the left) and at 90° (on the right)	35
Figure 26: Current x Phase for the monitor	36
Figure 27: Current x Phase for the DCPS	36
Figure 28: Monitor circuit.....	37
Figure 29: DCPS circuit	37
Figure 30: Validation for the monitor at 0°	38
Figure 31: Validation for the monitor at 90°	38
Figure 32: Validation for the DCPS at 0°	39
Figure 33: Validation for the DCPS at 90°	39
Figure 34: Error for the monitor in phase 0°	40
Figure 35: Error for the monitor in phase 90°	40
Figure 36: Error for the DCPS in phase 0°	41
Figure 37: Error for the DCPS in phase 90°	41
Figure 38: A single phase source with a variable resistor	48
Figure 39: Output voltage and current on the resistor	48
Figure 40: A single phase source with a varistor	49
Figure 41: Output voltage and current on the varistor	50
Figure 42: 1 st DCPS VWCB receiver modules (B-Cabinet).....	51
Figure 43: 2 nd Optical DL DVI splitter (B-Cabinet)	51
Figure 44: Dual Link splitter (B-Cabinet)	51
Figure 45: 2 nd DCPS VWCB receiver modules (B-Cabinet)	52
Figure 46: 3 rd DCPS VWCB receiver modules (B-Cabinet)	52
Figure 47: 2 nd MCS monitors (WME 1.8) (M-Cabinet)	52
Figure 48: CRCB continuous (M-Cabinet).....	53
Figure 49: CRCB switched (M-cabinet)	53
Figure 50: 16x16 DVI matrix switch (B-cabinet)	53
Figure 51: SIB (M-cabinet)	54
Figure 52: Host PC (M-Cabinet).....	54

Figure 53: IP PC F (M-Cabinet).....	54
Figure 54: IP PC L (M-Cabinet).....	55
Figure 55: Flexvision Dell PC (B-cabinet).....	55
Figure 56: Tube Cooler F (M-Cabinet)	56
Figure 57: Tube Cooler L (M-Cabinet).....	56
Figure 58: 1 st DCPS VWCB receiver modules.....	57
Figure 59: 2nd Optical DL DVI splitter	57
Figure 60: Dual Link Splitter	58
Figure 61: 2 nd DCPS VWCB receiver modules.....	58
Figure 62: 3 rd DCPS VWCB receiver modules.....	58
Figure 63: MCS Monitor	59
Figure 64: CRCB Monitor.....	59
Figure 65: 16x16 DVI matrix switch.....	60
Figure 66: SIB.....	60
Figure 67: Host PC	60
Figure 68: IP PC F	61
Figure 69: IP PC L	61
Figure 70: Flexvision Dell PC.....	61
Figure 71: Tube Cooler F	62
Figure 72: Tube Cooler L	62
Figure 73: Monitor (power switched in phase 0°)	63
Figure 74: Monitor (power switched in phase 30°)	63
Figure 75: Monitor (power switched in phase 60°)	63
Figure 76: Monitor (power switched in phase 90°)	64
Figure 77: Power Supply (power switched in phase 0°)	64
Figure 78: Power Supply (power switched in phase 30°)	64
Figure 79: Power Supply (power switched in phase 60°)	65
Figure 80: Power Supply (power switched in phase 90°)	65

Figure 81: Monitor (power switched in phase -30°).....	65
Figure 82: Monitor (power switched in phase -60°).....	66
Figure 83: Monitor (power switched in phase -90°).....	66
Figure 84: Power Supply (power switched in phase -30°).....	66
Figure 85: Power Supply (power switched in phase -60°).....	67
Figure 86: Power Supply (power switched in phase -90°).....	67
Figure 87: Monitor Phase 0°	67
Figure 88: Monitor Phase 30°	68
Figure 89: Monitor Phase 60°	68
Figure 90: Monitor Phase 90°	68
Figure 91: Monitor Phase -30°	69
Figure 92: Monitor Phase -60°	69
Figure 93: Monitor Phase -90°	69
Figure 94: DCPS Phase 0°	70
Figure 95: DCPS Phase 30°	70
Figure 96: DCPS Phase 60°	70
Figure 97: DCPS Phase 90°	71
Figure 98: DCPS Phase -30°	71
Figure 99: DCPS Phase -60°	71
Figure 100: DCPS Phase -90°	72

LIST OF TABLES

Table 1: Loads Errors.....	43
Table 2: Monitor and DCPS Errors.....	45

LIST OF ABBREVIATIONS

AC	Alternate Current
DC	Direct Current
DCPS	Direct Current Power Supply
DL DVI	Dual-Link Digital Visual Interface
LSO	Load Side Option
MCS	Monitor and Control Software
MMF	Magnetomotive Force
PCM	Power Control Manager
PDM	Power Distribution Manager
PDS	Power Distribution System
PE	Protective Earth
PPB	Pulse Power Bus

ASSIGNMENT DESCRIPTION

Philips Healthcare is a company responsible to develop and market solutions that promote wellness for people around the globe. The Healthcare sector's vision is to improve the quality of patients' lives by simplifying the delivery of healthcare, improving clinical outcomes and reducing healthcare system costs around the world [1]. The Power Distribution System (PDS) project is executed within the Research and Development department of the business unit interventional X-Ray. This department is specialized in the development imaging equipment for interventional imaging, treatment and clinical research.

This study is about a new power distribution architecture that is intended to be scalable and applicable for powering medical facilities with imaging equipment. Part of the system is already finished, but there is still an amount of loads that needs to be tested. Therefore, the aim of this assignment will be focused on the load models and their parameterization. It will involve application and verification activities for the created models (in LTspice software), executing the models in order to yield predictions about the outcome of real life verification measurements. After data collection and analysis, it will be necessary to feed the information back into the model, in order to have improvement in the accuracy and, if applicable, apply the necessary corrections into the models.

The Spice models that were developed are based on the flow of power within the power system. The electrical power that comes through the lines distributions flows into the hospital mains over the Power Distribution System (PDS). The PDS is an architecture that has been concept by Philips Healthcare after years of research. This architecture consists of a power distribution platform for medical purposes composed by building blocks model interfaces [3]. The schematic, shown in Figure 1, illustrates the flow of power from the hospital mains until the load.

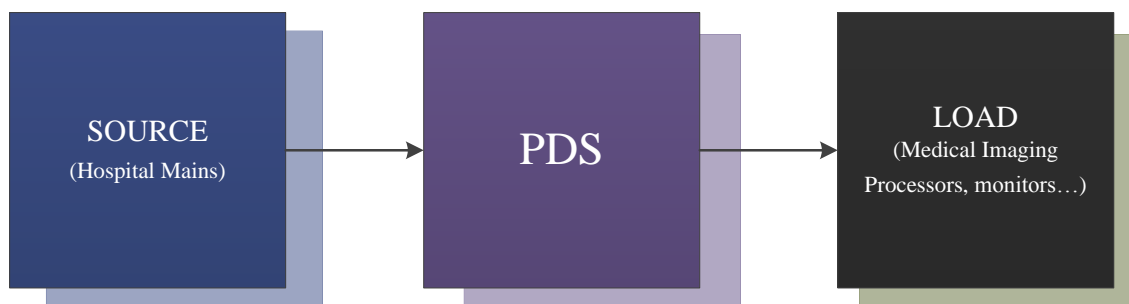


Figure 1: Power Flow Diagram

Considering the PDS structure, it can be divided in three main parts.

- 1) **Power Control Manager (PCM) Domain:** The central domain that converts, switches, distributes, buffers and monitors the power. The distribution constitutes in partitioning in to power bus (**PDS.IF.PB**) and pulse-power-bus (**PDS.IF.PPB**) root terminals. It converts a 400/230V Wye configuration into the power-bus and 380-480V. It switches on/off the output power of the PB and PPB roots. By buffering, it stores the energy in batteries and use the energy to continue providing output power in case of lost power in the source.

- 2) **Power Distribution Manager (PDM) Domain:** The PDM is a slave of the PCM master controller. It converts a three phase in to a single-phase and phase association section. It taps the switching of single phase loads and splits off into multiple and identical tap channels. It stores the energy in batteries in order to provide output power in case of lost power in the source.

- 3) **Load Side Option (LSO) Domain:** This domain is responsible to distributes, converts and conditions the power in physical proximity of the load. All functions are intended to adapt the PDM.

The power will flow through the hospital mains to the PDM. After entering the PDM, the power will be split into two paths. One path is the 3 Phase Pulse Power Bus (PPB), which will distribute the power to the Medical Imaging Processor. The other path is the 3 Phase Power Bus with UPS (PB), responsible for the power distribution for the single phase tap switching units, which can be paralleled towards multiple single phase loads. In this path, there may also be a connection from the tap switch to a DC load via a Load Side Option (LSO). The PDS has the main purpose of mitigate distortions deriving by the power source. The schematic of this system is illustrated by Figure 2.

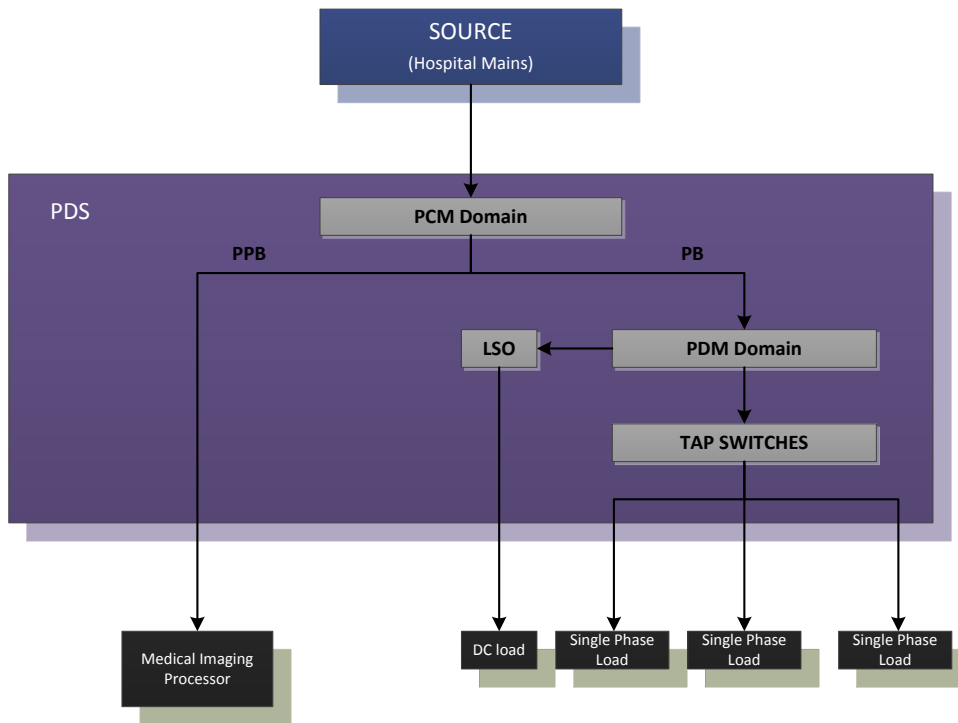


Figure 2: Power Distribution System Schematic

Due to limitations of time, it was only possible to develop a model for the AC loads. This way, further studies can be done with the DC and the three-phase delta loads in order to complete the architecture. This project will describe the different load models simulated in LTspice and the measurements with real loads in the X-Ray laboratory. At the end, the results will be validated to see how close the models are from the real loads.

1. INTRODUCTION

The PDS is a big architecture whose performance is difficult and complex to test. The best way to verify the system's performance is through simulation, once it enables to check the results beforehand and helps to get information of the system's behavior without testing it in real life. However, the process of designing this architecture, as well as simulating the loads connected to it, involves a deep understanding of the load's electronic circuit that causes a certain behavior when the voltage is switched on. Understanding this behavior is the goal of this study because we are mostly interested in the current that is generated when the device is first turned on. These currents, usually called inrush currents, have a huge influence on the device's operation life since they exceed the steady-state current value.

The models designed in LTspice software were based in the power flow diagram that was shown in Figure 1. It means that the electrical circuits' models present, in a simple way, the switch mode power supply, the PDS and the load. The power supply was designed in a way that it can be switched on at any time, according to the configurations set by the user. The phase of the voltage waveform can also be changed in order to understand its influence on the inrush current peak value. The variable parameters that describe the circuits are set in specific values in order to simulate specific loads. Each load has a fixed value for each parameter, and these values were carefully tested to approach the result most similar to the lab result for that load.

This report contains the activities that were done, the obstacles encountered, the solutions defined and the results that were found. In this first chapter, a brief introduction to the power distribution system is given for a clearer understanding of the entire process. Moreover, there will be a section explaining the inrush current, since it's the main phenomenon that we are interested in. Explanations about how the models were created are found in chapter 2, Load Building Model, and the laboratory measurements and analysis can be found in chapter 3, Practical Analysis. The results and discussion are in chapter 4 and finally, the conclusions are written on chapter 5. A lot of practical results were left outside the main part of the report, but they can be found on the appendices.

Finally, it's important to emphasize that all of the computational models created were based on the current and voltage waveforms contained on the characterization report of 2013, with the exception of the DCPS and the monitor, that were based on our own measurements in the lab. All of the measurements and the resulting graphs can be found on the Appendices B and C.

1.1 Electric Power Distribution System

The three-phase electric power is a method of alternating-current power generation, transmission, and distribution. Figure 3 shows this polyphase system, which is the most common method used by electrical grids worldwide to transfer power. A three-phase system is usually more economical than an equivalent single-phase or two-phase system because it uses less conductor material to transmit electrical power [4].

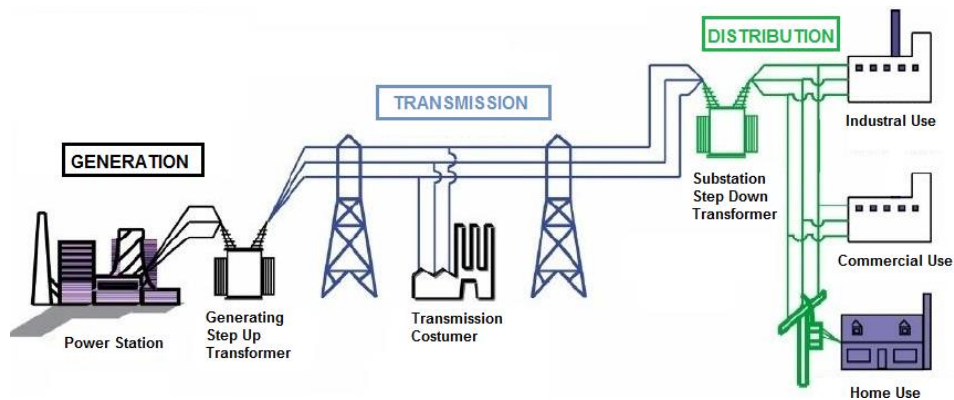


Figure 3: Overview of Electrical Distribution System

At the power station, an electrical generator converts mechanical power into a set of three AC electric currents, one from each winding of the generator. The windings are arranged such that the currents vary sinusoidally at the same frequency (50 Hz in the Netherlands) but reach their instantaneous peak values at one third of a cycle from each other. Taking one current as the reference, the other two currents are delayed in time by one third and two thirds of one cycle of the electric current (Figure 4). This delay between phases has the effect of giving constant power transfer over each cycle and also makes it possible to produce a rotating magnetic field in an electric motor.

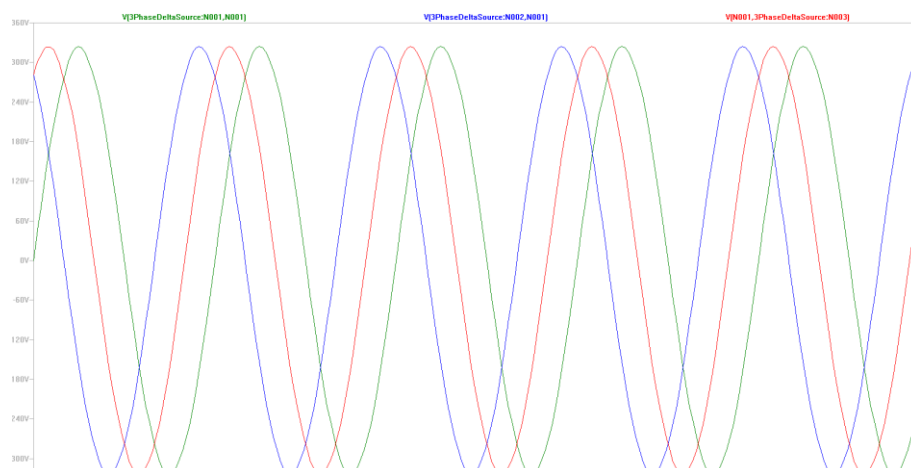


Figure 4: Three phase AC waveform

Generating step up transformers change the voltage from generators to a higher level suitable for transmission in order to avoid losses during transmissions. These voltages are extremely high, producing low currents and therefore less power loss.

After transmission, the step down transformer reduces the primary voltage to a level where it can be used by the end costumers, which can be, for instance, an industry, the hospital mains or houses. In the latter, it is a three-phase to single phase conversion and it's referred to as a delta-to-wye conversion.

All of the electrical power that comes out from this distribution system and enters the hospital mains flows into the PDS, as shown in the schematic in Figure 1. At the end, the electrical power that is out of the PDS will be connected to different medical equipment which will be defined as the load for this assignment.

1.2 Inrush Current

In order to power these medical appliances, one should take into account the safety requirements and the maximum allowable currents that a specific device can tolerate without any damages. The maximum and instantaneous input current drawn by an electrical device when power is first applied is called inrush current and it can affect electrical components inside a circuit and failure within the equipment itself.

The inrush current is greater than the nominal operating current of the equipment and its value varies according to the equipment in question and the state of operation. It can range from 5 to 100 times greater the normal full load current.

The figure below shows an example of an inrush current from one of the loads tested in the laboratory, the DCPS VWCB receiver module.

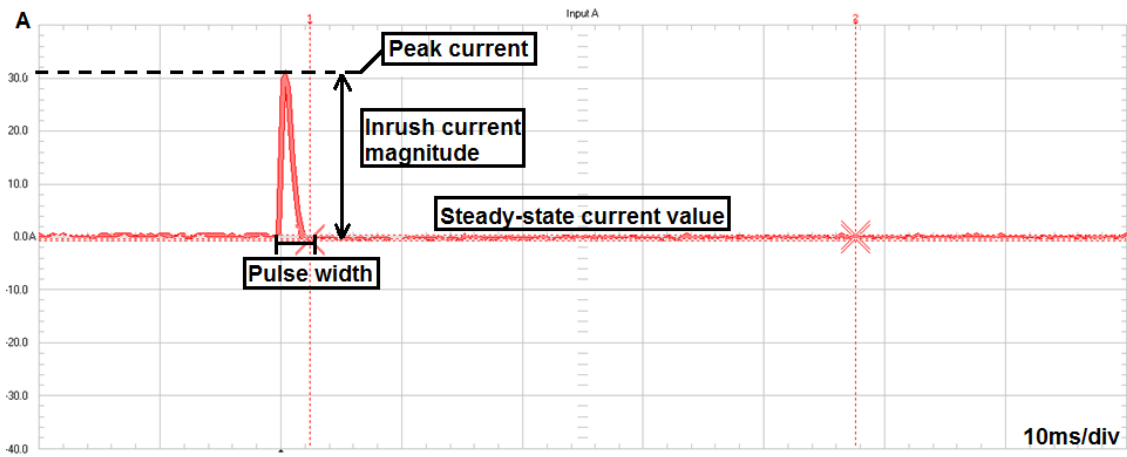


Figure 5: Current waveform when the device is powered up

When the power is turned on, current begins to flow, and the initial current flow reaches the peak current value that is larger than the steady-state current value. Following this, the current value gradually decreases until it stabilizes at the steady-state current. The part during which a large current flows before reaching the steady-state current is the inrush current. If the size of the inrush current exceeds that allowed by the part in use, depending on the magnitude of the inrush current (difference between the peak current value and the steady-state current value) and length of its duration (the length of time until the peak current value converges with the steady-state current value, hereafter called the pulse width), the part used in the circuit may overheat, potentially causing the electrical device to malfunction or break down.

The reasons why this inrush current occurs vary according to each device. In general, in equipment with large-capacity smooth capacitors or decoupling capacitors, when the power is first turned on, a large current flow to charge those capacitors – a necessity when first powering up the equipment. Another reason is that immediately after the power is turned on, the filament and other parts have low resistance, so large current flows. As they begin to generate heat and warm up, the resistance increases and the current drops to the steady-state current.

If the load is connected to an AC powered source, the maximum inrush is dependent on the point on the AC waveform at the time it is switched on [5]. As it will be seen later on this report, the load may be connected when the mains waveform passes through zero or at the very peak of the voltage waveform. It can also be connected between the two points, but mostly it will be somewhere between the two extremes, and the cycle could be positive or negative.

Transformers and other inductive circuits behave in a manner that is not intuitive. In a transformer, for example, the greatest magnitude of inrush current occurs at the zero crossing of the terminal voltage, whereas the lowest magnitude occurs when the power is connected at the peak of the AC voltage waveform. This is because at the zero crossing the flux saturates the core and a high amplitude inrush current appears, since the inductance of the magnetic core is very small in that region. Therefore, the peak current is only limited by the circuit resistance and the current is determined by Ohm's law.

Since it is not possible to choose when power is applied, any provision for inrush current must assume the highest possible value.

2. MAGNETIC COMPONENTS

Due to the presence of the magnetic components in many power electronic equipment of the PDS, a certain time of this internship was dedicated to study more deeply this kind of devices. Although LTSpice offers a few magnetic components built into it, the most reliable way to create these models is to base them on the actual physical structure of the component. It means, for example, that a transformer won't be represented by a coupled inductor model, but by a circuit that mimics the behavior of the transformer. Therefore, the physical structure of the device needs to be translated into an equivalent electric circuit [6].

To make a transformer model that more closely represents the physical processes, it is necessary to construct an ideal transformer and model the magnetizing and leakage inductances separately. The SPICE equivalent circuit for an ideal transformer is shown in Figure 6, and it implements the following equations:

$$V1 \cdot \text{ratio} = V2$$

$$I1 = I2 \cdot \text{ratio}$$

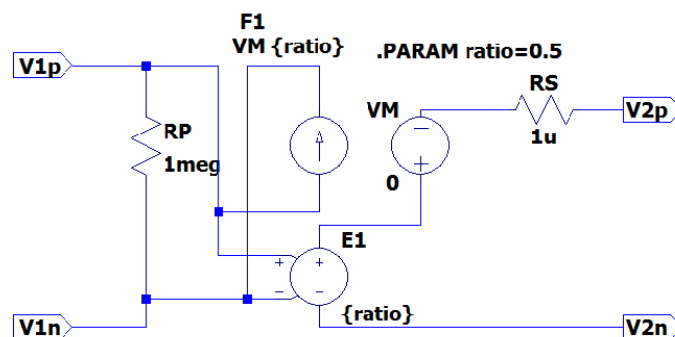


Figure 6: The electric circuit of an ideal transformer

In the circuit above, the voltage-controlled voltage source is set with the turns ratio from the windings and the resistances R_p and R_s are used to prevent singularities in the matrix used by SPICE to calculate the voltages and currents.

The nonlinear characteristics of the transformer are performed by another electric circuit shown in Figure 7. It represents a single coil wound around a magnetic core, which is consisted of many magnetic domains made up of magnetic dipoles. These domains set up a magnetic flux that adds to the flux that is set up by the magnetizing current. In the presence of an applied field, the domains rotate until they are all in alignment with the field and the core saturates.

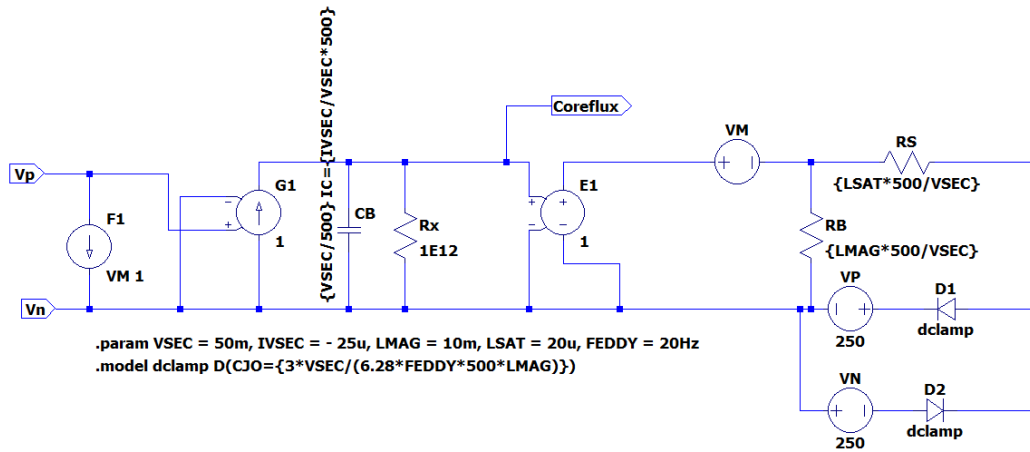


Figure 7: Equivalent electric circuit of saturable core model

Modeling the nonlinearities of a transformer is more easily accomplished by adding nonlinear elements to the model. In this case, the diodes are responsible for causing the expected behavior of the transformer, making it possible to plot the B-H loop hysteresis curve. The capacitor C_b is described by an initial condition that allows the core to have an initial flux, whereas resistors R_b and R_s are responsible for the inductance in the high-permeability region and the saturated region, respectively. The voltage sources V_n and V_m represent the saturation flux and R_x simulates the core losses, which increase linearly with frequency.

The characteristics of the core are determined via the specification of a few parameters:

- Flux capacity in volt-seconds (VSEC)
- Initial flux capacity in volt-seconds (IVSEC)
- Magnetizing inductance in henries (LMAG)
- Saturation inductance in henries (LSAT)
- Eddy current critical frequency in hertz (FEDDY)

The values attributed to each parameter were calculated in order to find compatible results with magnetic components' behavior. These values can be seen as a SPICE directive on LTSpice schematic on Figure 7.

The saturable core is added to the model of the ideal transformer to create a complete transformer model. It is a piece of magnetic material with a high permeability used to confine and guide magnetic fields in electrical and magnetic devices such as transformers, electric motors, inductors and magnetic assemblies. The high permeability, relative to the surrounding air, causes the magnetic field lines to be concentrated in the core material. The magnetic field is often created by a coil of wire around the core that carries a current. The presence of the core can increase the magnetic field of a coil by a factor of several thousand

over what it would be without the core. The use of a magnetic core can enormously concentrate the strength and increase the effect of magnetic fields produced by electric currents and permanent magnets.

Figure 8 shows the top subcircuit level, where a special test point has been provided to allow the monitoring of the core flux during simulation. The voltage source is a sine-wave excitation with a frequency of 50Hz and varying amplitude, in order to see the effect of the wave over the B-H hysteresis curve.

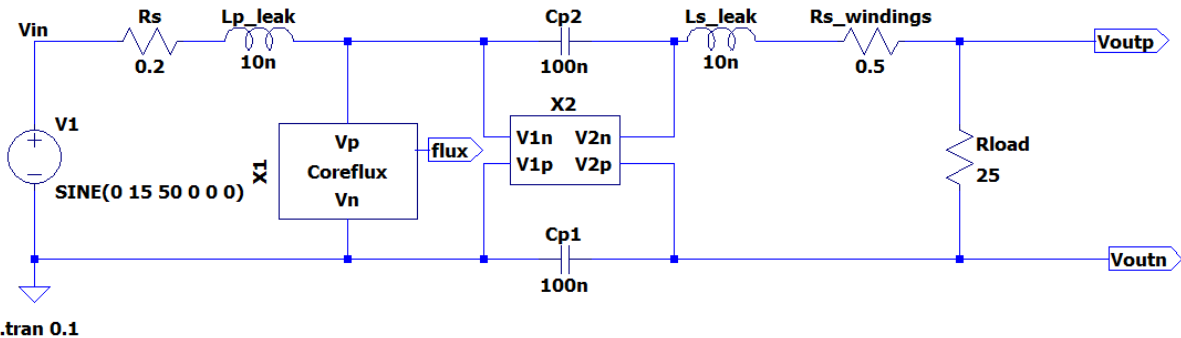


Figure 8: Complete transformer model

In the circuit above, X1 is the core model and X2 is the ideal transformer. The complete model also has a leakage inductance and the windings resistance in series with the inductance. A stray capacitance with parallel resistance is required to prevent the matrix to become singular. The results obtained when both circuits are combined are presented in Figure 9.

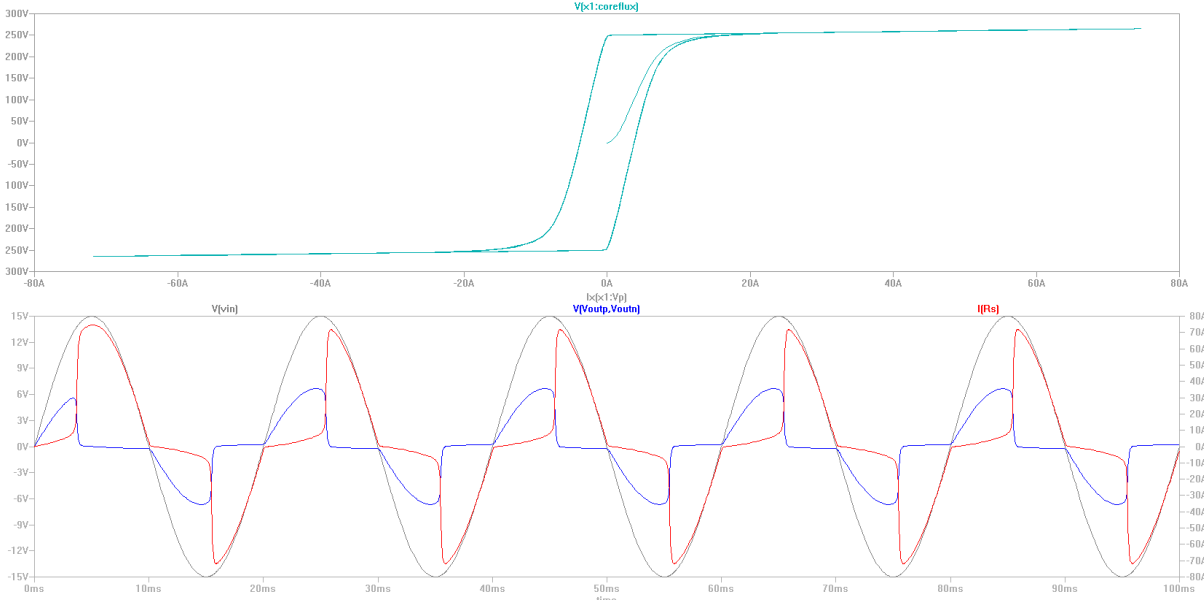


Figure 9: The result when simulating the complete transformer model

In the first graph, the light blue curve represents the magnetic intensity field and magnetic flux density plot. When the magnetic field through the core changes, the magnetization of the core material changes by expansion and contraction of the tiny magnetic domains it is composed of, due to movement of the domain walls. This process causes losses, because the domain walls get snagged on defects in the crystal structure and then snap past them, dissipating energy as heat. This is called hysteresis loss. It can be seen in the graph of the B field versus the H field for the material, which has the form of a closed loop. The amount of energy lost in the material in one cycle of the applied field is proportional to the area inside the hysteresis loop.

The second graph shows the input voltage (in gray), output voltage (blue) and the current through the core (red). When the core reaches the saturation, the losses become larger, affecting directly the output voltage and deforming characteristically the sinus waveform. The distortion of the sine wave is more perceptible in the zero-crossing points of the voltage source, where the derivative $\frac{dV(t)}{dt}$ is maxim. In these points, the core saturates easily, stressing the transformer and causing dissipation of energy in the core, and not on the load.

If we now change the amplitude of the source the dependence of the saturation on the voltage becomes clearer. Increasing the voltage amplitude causes an increase in the magnetomotive force (MMF), which in turn causes a larger magnetic flux and the core saturates easier. To visually represent this relation, Figure 10 shows three examples where the amplitude of the input voltage was varied.

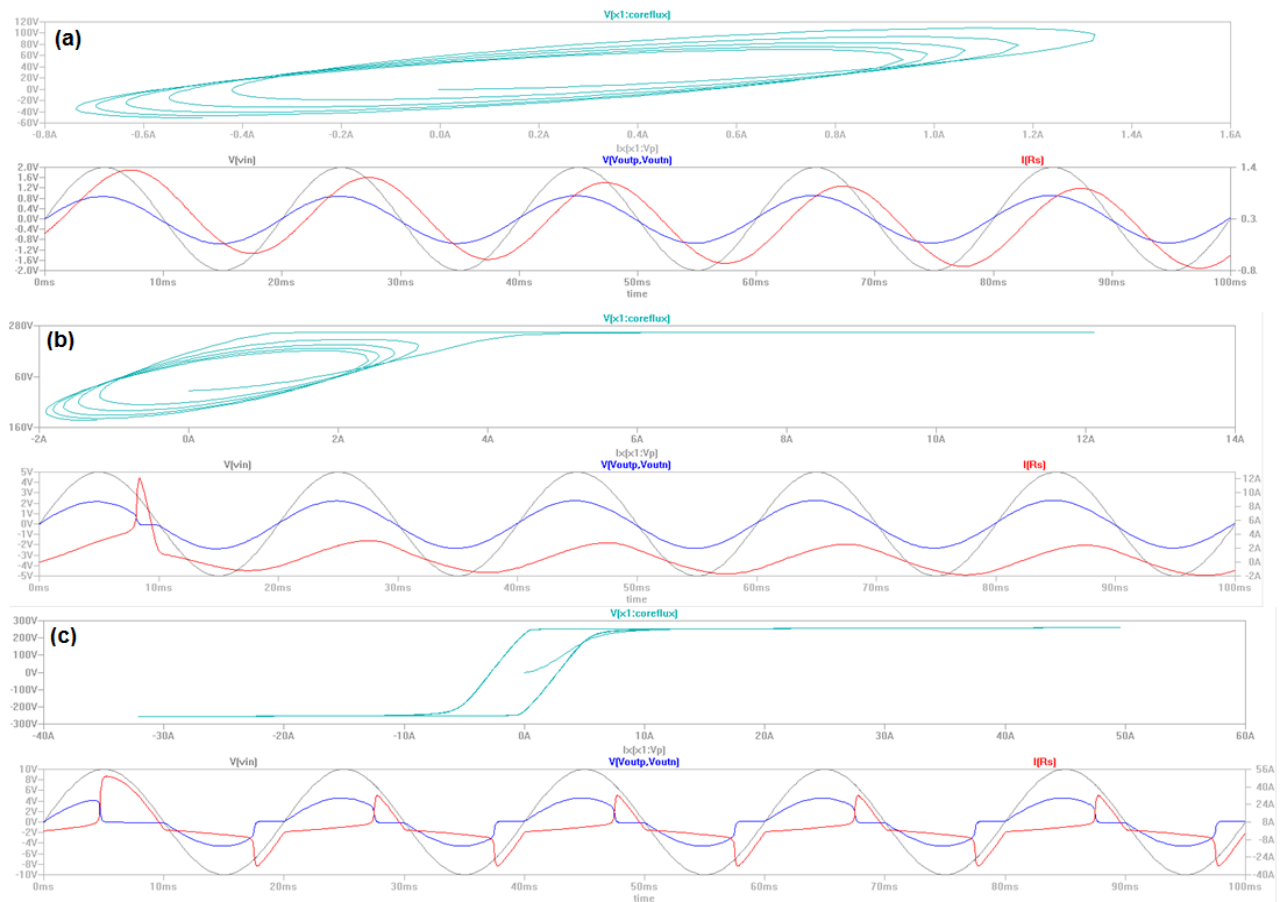


Figure 10: Results obtained when the amplitude of the input voltage source was varied and set as (a) 2 volts, (b) 5 volts and (c) 10 volts

In the first figure above, letter (a), the hysteresis curve shows that the core is not saturated yet. Both the output voltage on the load and the current are a perfect sine waveform, indicating that the core losses were not large enough to distort the load voltage waveform. The second, figure (b), represents a situation where the core just started to saturate. There is a clear peak on the current right in the beginning of the simulation, followed by a slightly distortion on the output voltage. The hysteresis curve, in this case, starts to show characteristics of a saturated core. Finally, the last graph, represented by the letter (c), shows a saturated core.

Another important parameter that influences the magnetization of the core is the phase at which the voltage is switched on. If it is switched at the phase of 90° , the rate of variation of the voltage is minimum, since $\frac{dV(t)}{dt}=0$. Two situations are shown in the figure below. In the first one, the source was switched on at phase 0° , whereas in the second one, at the phase 90° . Both of them have the same voltage amplitude of 5 volts.

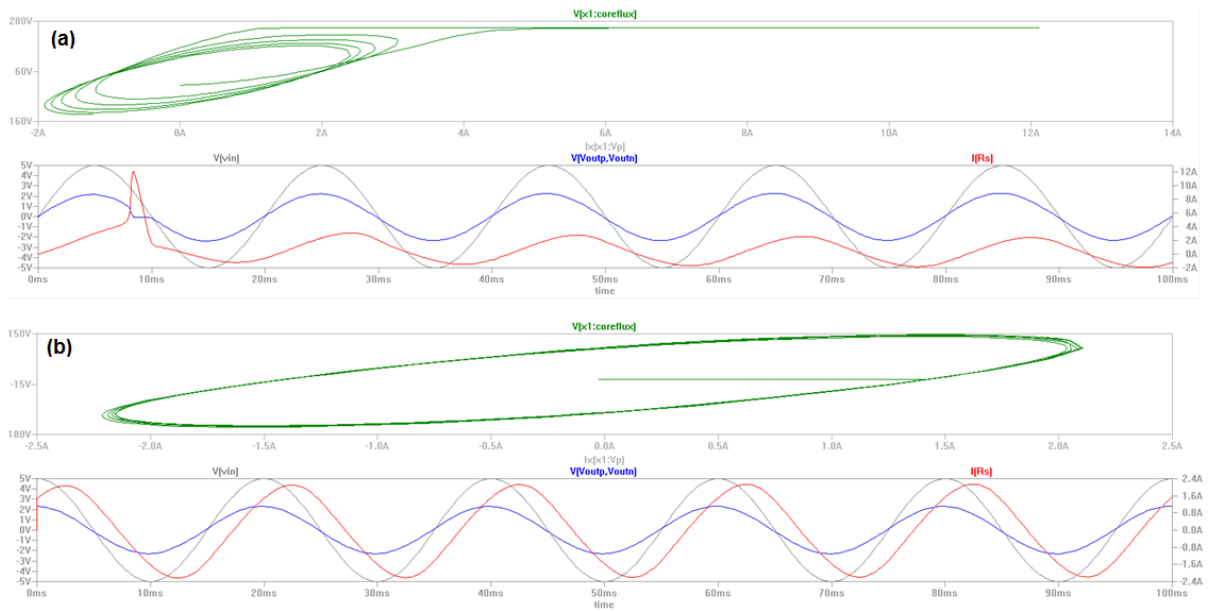


Figure 11: Hysteresis curve and output voltages and current obtained with the source switched on at (a) 0° and (b) 90°

As seen before in Figure 10b, the first graph shows a situation where the core is saturated. The inrush current present in the graph is due to the power that was first applied with the AC source at the zero-crossing point. This peak is not present in the second graph, where the source was switched on at 90° . In this case, the transformer is not saturated, even connected to a source with the same amplitude. The hysteresis curve has an interesting behavior: its initial magnetizing curve is a horizontal line. It means that there is an increase in the magnetic flux, even with no increase in the intensity of the magnetic field.

Avoiding high magnitudes of inrush current is extremely important in the protection of electronic devices. This is the reason why control switching is so important: the inrush current can be minimized when powering a transformer at the maximum peak voltage (90°).

Although the models built so far properly represent the nonlinear permeability and the hysteresis, there was still one model left that was not simulated due to time limitations. This model represents low-frequency hysteresis in transformers, and can be studied by the next team that will take this project.

3. LOAD MODEL BUILDING

Appropriately modeling load characteristics is important for power distribution analysis, in particular for presuming the behavior of the system when the load is connected to it. It is not an easy task, since the sensitivity of the system behavior to changes in load response must be clearly understood.

In order to improve the process and accuracy of the PDS and to be able to make rational and economical decisions, a verification tool is needed to facilitate and to reduce the costs of testing. LTspice was the software used to acquire the necessary characteristics and parameters with respect to the various kinds of loads in the power system, such as the PCs, the monitors and the X-ray machines.

The result of the simulations developed in LTspice led to a better understanding of the load dynamics and therefore to an improved load representation, making it possible to decrease uncertainty margins, resulting in a positive impact on the reliability of the system operation.

1.3 Software Simulation

LTspice IV is a high performance SPICE simulator, schematic capture and waveform viewer with models for easing the simulation of switching regulators. The benefit of using a simulator is that it provides us a guideline for expected results in the laboratory. It is also useful for purposes of comparison between what was observed in the software and what was seen in the practical measurements. This way, it's possible to verify if models created are following real life expectations.

The modeling of the load has started with some simple resistive, RL, RC, and RLC single phase loads simulations, providing not only the circuits behavior analyses, but also an easy way to improve the skills with the software's tools. After this initial contact with LTspice, the main focus on the load design was to turn the computational model as close to a real load behavior as it could.

In the hospital, more specifically in an X-Ray room, three phase (e.g. the X-Ray generator) and single phase (e.g. monitors) loads are connected to the power distribution system. Although the simulation of the original circuits of this kind of load provides more reliable results, the time to simulate them becomes inappropriate. Therefore, it's necessary to look for a solution that provides good results in a short period of time.

In order to visualize one of the most expressive behaviors of the load, the inrush current, a few techniques to vary the impedance of the computational load model were applied. In the beginning, a single load was designed using first a variable resistor and then using a varistor. In both cases, the results were not so meaningful and it will be discussed on the Appendix A – Load Modeling.

The second step taken was to impose a mathematical function that could describe the inrush current in a resistive component. Thus, a resistor was described as growing exponential damped over time, as illustrated in Figure 12.

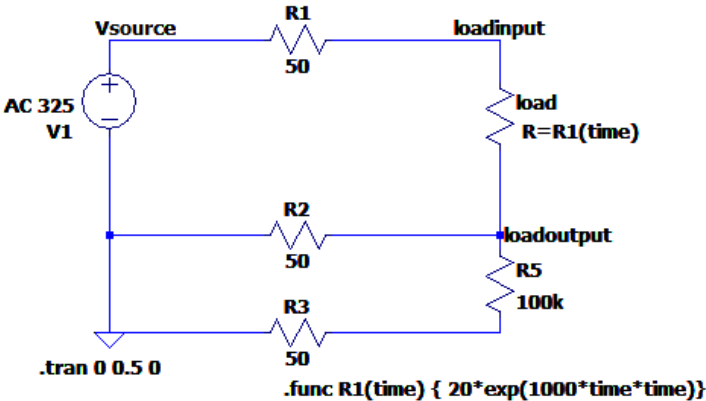


Figure 12: Single phase load described as a mathematical function

The schematic represented by Figure 12 illustrates in a simple way a single phase load supplied by an AC voltage source, connected to a power distribution unit (represented by the resistor R1). The resistors R2 and R3 represent, respectively, the neutral and the Protective Earth (P.E). The high resistance value of R5 ensures that no current runs through the P.E. Through LTspice simulation, the voltage at the source and the current at the load are presented in Figure 13.

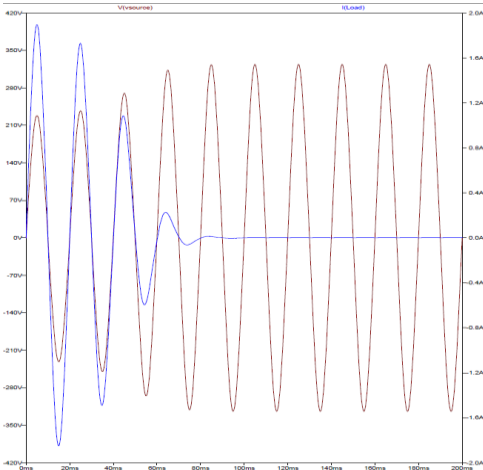


Figure 13: Voltage at the source and current at the load

In the PDS, the measurements can be done in three different cabinets: B, M and R. For each one of these cabinets, different types of loads have been tested, having their current waveform displayed in the scopemeter. Once the representation of the resistive load as a function of time was successful, the next step taken was to establish for the B and M cabinets (for a matter of time, only these two were analyzed) types of loads that have similar behavior in order to parameterize them. The loads have been allocated in six groups that hold similar characteristics, providing an easy way of modeling and parameterization. Through the loads characterization and with LTspice support, each type of load was described as function of time supplied by a switch mode power supply hooked up through resistors that represent the losses in the transmission line.

One example of the inrush current for each type is shown below and the complete list of load type can be found in the Appendix B - Load Types.

✓ Type A

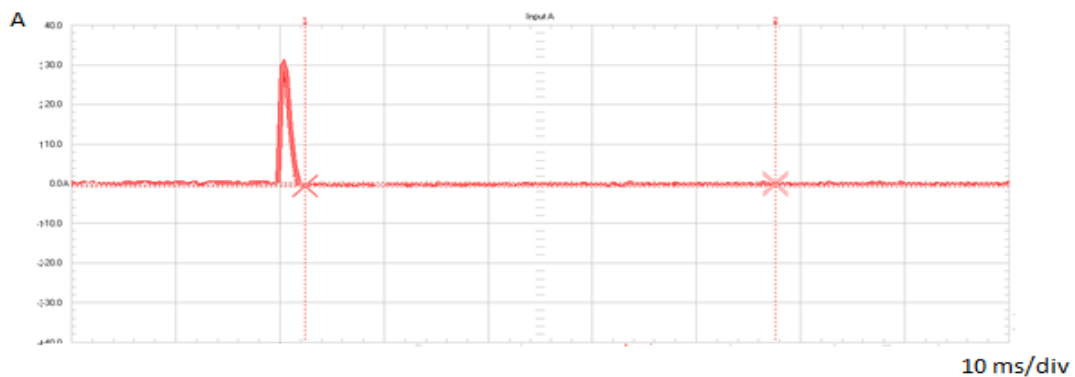


Figure 14: DCPS VWCB receiver modules (B-Cabinet)

✓ Type B

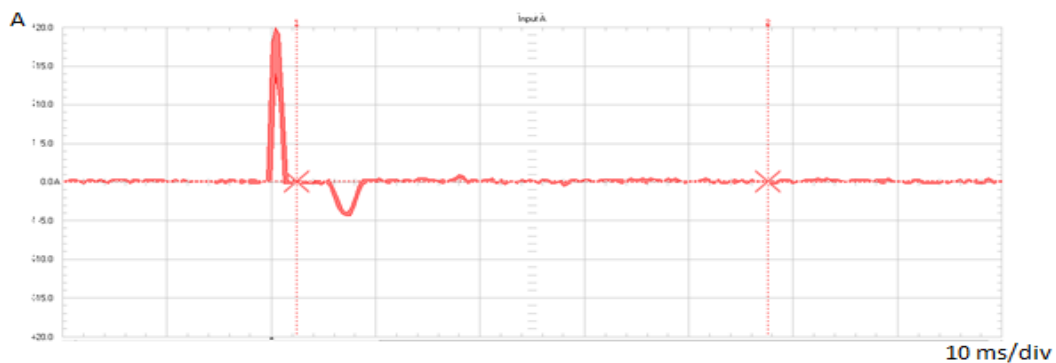


Figure 15: DCPS VWCB receiver modules (B-Cabinet)

✓ Type C

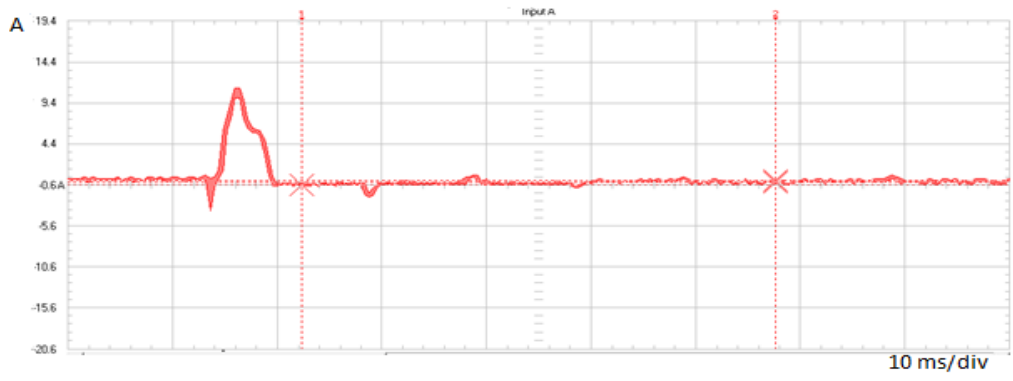


Figure 16: CRCB continuous (M-Cabinet)

✓ Type D

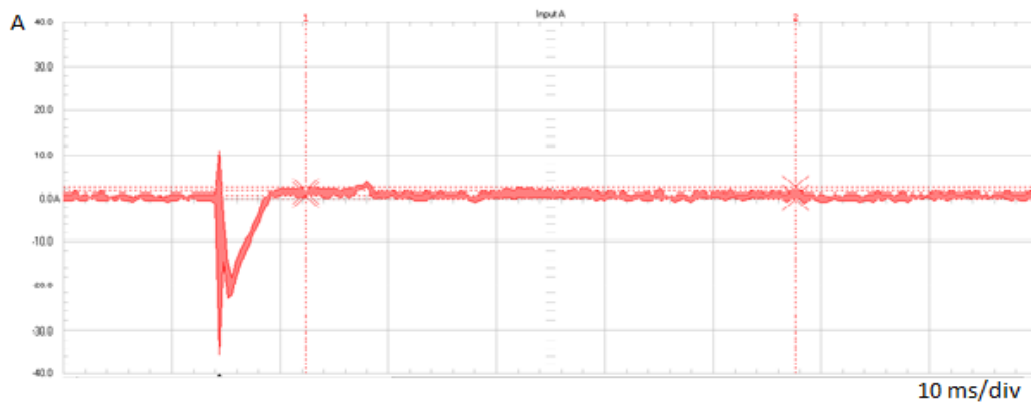


Figure 17: SIB (M-cabinet)

✓ Type E

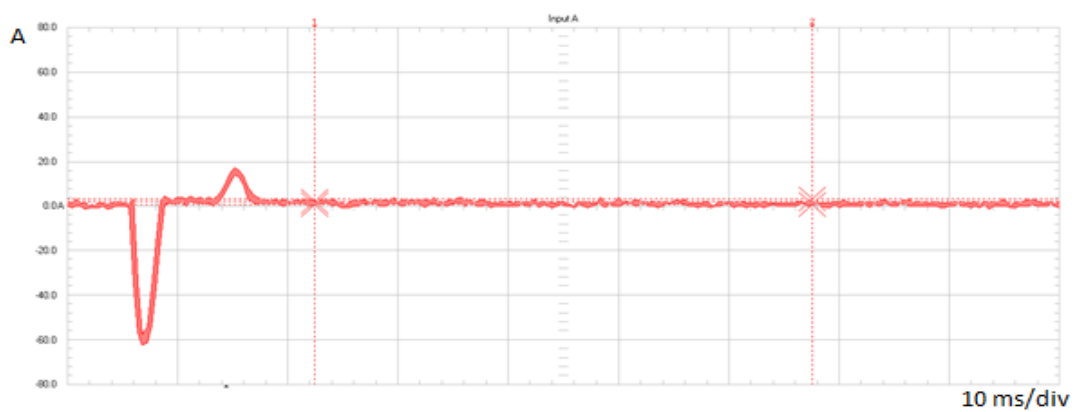


Figure 18: Host PC (M-Cabinet)

✓ Type F

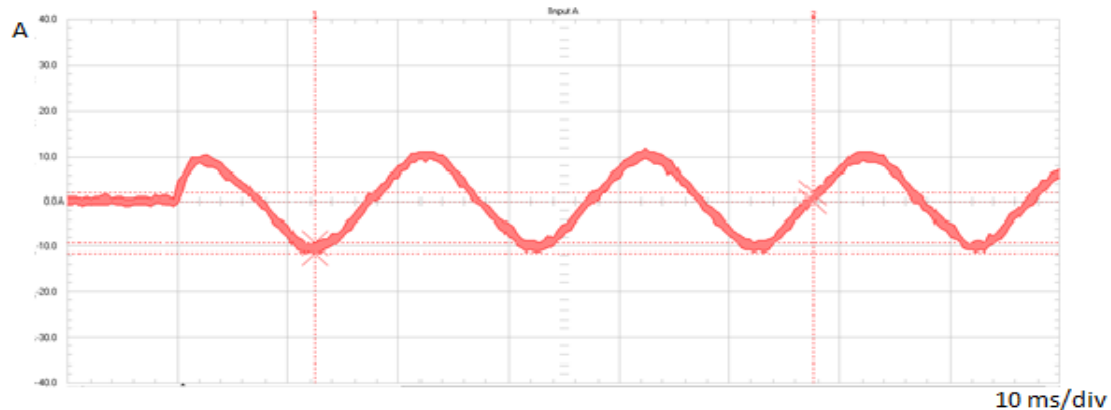


Figure 19: Tube Cooler F (M-Cabinet)

It is remarkable that loads of types A to E present a similar inrush behavior – all of them present a huge first peak that is sometimes followed by other smaller peaks before it reaches the steady-state current. This is due to the presence of the DC Power Supply (DCPS) in these circuits. Loads of type F, on the other hand, have an inrush current behavior that is similar to a sinusoidal waveform, presenting some shifting, that persists from the beginning to the end. This characteristic is based on that the tube cooler (a type F load) is composed by some inductive components (e.g. the fan and the motor) that may shift or distort the sine wave.

The difference observed between the current waveforms of loads from type A to E is caused by the many different components inside the DCPS. In a typical power supply, the AC input voltage deriving of the mains power is stepped down to a desired level using a transformer. When it is already stepped down, AC voltage is connected to a rectifier diode that converts the AC voltage in to a pulsating DC. This conversion is based on the principle that a diode acts as a conductor with a very low resistance when forward biased, and acts as an insulator with a very high resistance when reverse biased. An electrolytic capacitor used for storing energy is usually connected across the DC output of the rectifier diode, providing an extra degree of smoothing the output waveform.

In general, all types of loads are represented by the same electrical circuit. What changes from group to group is the mathematical function that describes the resistor in the circuit, which represents the load. This way, it is possible to use the same mathematical function to simulate different loads that belong to a particular group, but the user must change the function's parameters when changing the load within that group.

The figure below shows the final model created with LTspice, in which the load is a resistor described as function of time, supplied by a switch mode power supply hooked up through resistors that represent the losses in the transmission line.

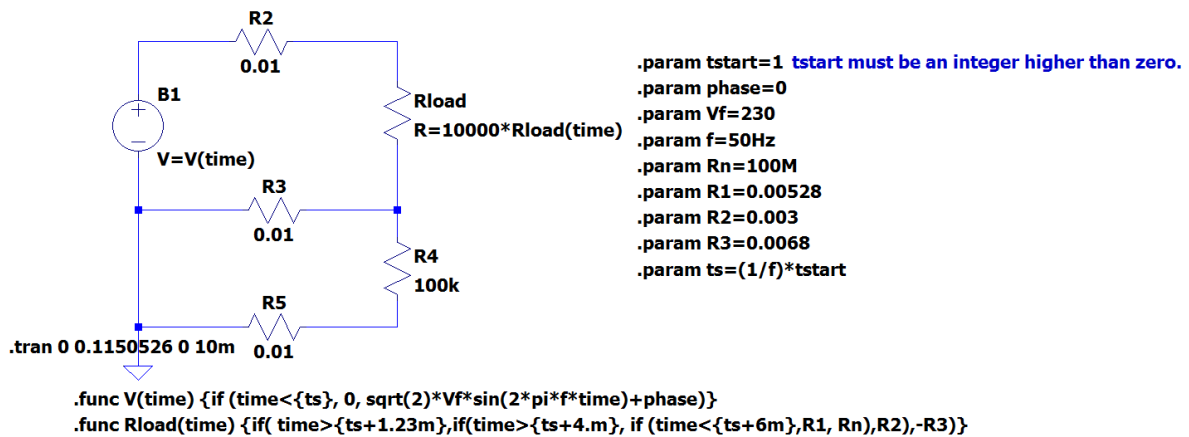


Figure 20: Circuit model (CRCB monitor)

The parameters defined can be changed by the user in order to obtain different loads characteristics. In the model, V_f represents the voltage amplitude of the mains power, f represents the frequency and $phase$ represents the phase of the sine wave. R_n , R_1 , R_2 and R_3 are the value of the resistor in different periods of time, and their values were attributed according to the desired amplitude for the current. Together, ts and $tstart$ assure that the switch moment is always on the zero-crossing. The user can change the value of $tstart$, but the voltage will always switch on when the sine wave is passing through the phase 0. In order to switch it on in a different phase, the user must change the parameter $phase$.

The resulting waveforms (current on the load and voltage on the source) from the circuit of Figure 20 are shown below:

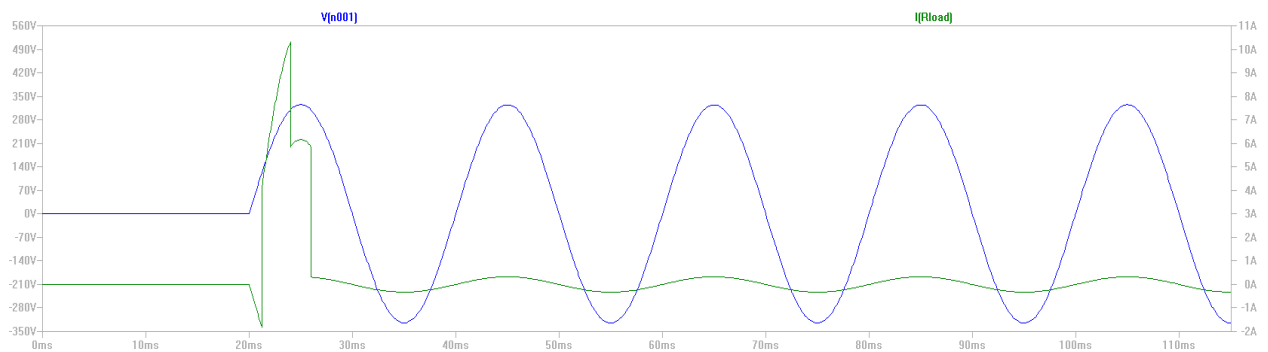


Figure 21: Simulation of CRCB monitor circuit model

It's clear that the variation of the resistor values causes the changes in the current waveform. The nominal value, R_n , is responsible for the steady-state current value and it was determined based on the characterization report of 2013. R_1 , R_2 and R_3 were first determined by Ohm's law and had their values increased or decreased until the right amplitude of inrush current was found. The pulse width was first measured in the Flukeview software and then written on the resistor function. Together, the parameters describe the function that simulates the behavior of the real load.

1.4 Data Interpolation

After the circuit simulation, the data from FlukeView (showing the original waveform) and LTspice were imported to an Excel file in order to validate the models through the error calculation between these two waveforms. However, not only the number of sampling points was different, but also the simulation time step of both softwares was not the same, making it difficult to calculate the error point by point. So in order to verify the accuracy of the model, an interpolation in the model's data became necessary.

First, the interpolation was done with the help of LTsputil, an utility software for LTspice which allows the user to change the numbers of sampling points and the simulation time step of the original LTspice file. The software automatically generates a new LTspice raw data file with the new parameters set by the user. In this case, the interpolation is based on the Polynomial Interpolation method, which from an amount of given points, finds a polynomial equation that fits exactly these points. However, this kind of interpolation became undesirable, since the waveforms got really distorted after the interpolation, losing the similarity with the real load behavior.

The other interpolation method applied to the models was the linear interpolation, using Excel as a tool. A linear interpolation is a simple method that assumes a straight line (linear) relationship between the known points, like shown in Figure 22. It essentially means averaging the two rates over the interpolation period.

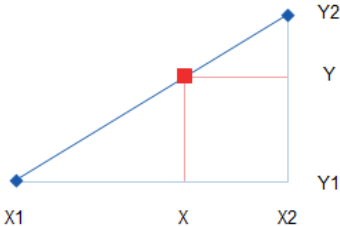


Figure 22: Linear interpolation between two points.

The diagram above shows two points (blue points connected by a blue line) with coordinates (X1, Y1) and (X2, Y2). In order to find the value of Y corresponding to a given X, represented by the red square at (X, Y), a simple algebra is necessary.

The smaller triangle with hypotenuse (X1, Y1)-(X, Y) is “similar” to the larger triangle with hypotenuse (X1, Y1)-(X2, Y2), so the sides of the triangles are proportionally sized, leading to the first equation below the sketch. Rearranging this to solve for Y:

$$\frac{X - X_1}{X_2 - X_1} = \frac{Y - Y_1}{Y_2 - Y_1}$$

$$Y = Y_1 + (X - X_1) * \frac{(Y_2 - Y_1)}{(X_2 - X_1)}$$

This was the final formula used for all the excel files for the different loads. With the linear interpolation, the resulting curve did not present an expressive difference from the original one, and thus, could be chosen without major losses in accuracy. Figure 23 presents the results obtained for the CRCB monitor. The graph is composed by three waveforms: the original data import from the scopemeter (FlukeView), the data import from the model created in LTspice and the interpolation of LTspice data.

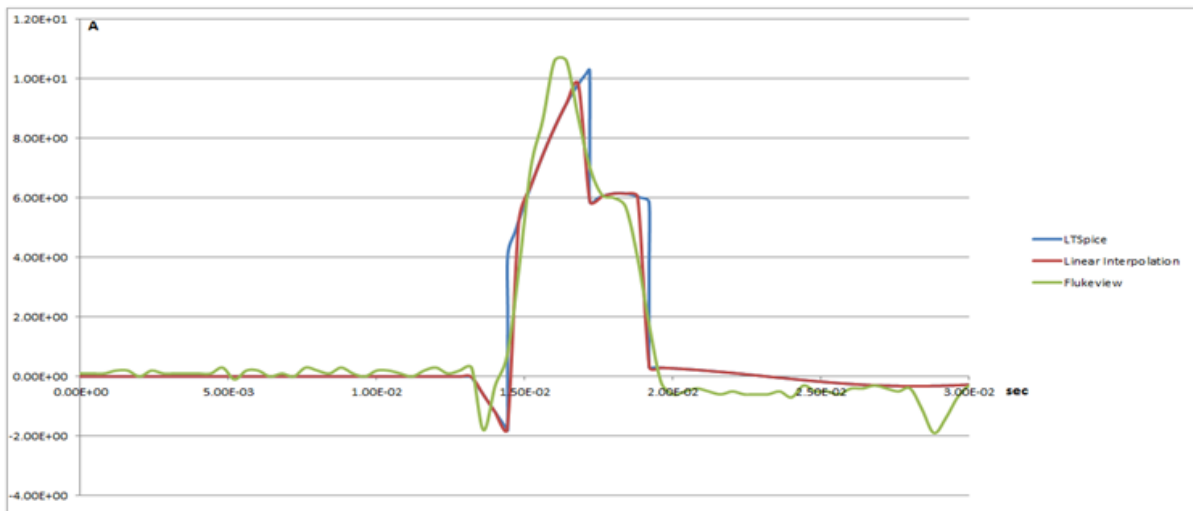


Figure 23: Validation CRCB monitor model

When importing the data from FlukeView to Excel, two different values for the current are given for the same time. They represent minimum and maximum values that are measured at a high sample rate, ensuring capture and display of glitches in the scopemeter. However, it is still not clear how two measurements are done at the same sampling time. In any case, the average value was used and plotted as the desired load behavior in all the simulations, even though the waveforms from the minimum, maximum and average values differed a lot from each other.

After plotting the Flukeview data based on the average values and interpolating the LTspice data, the next step was to calculate the error between these two curves. This was possible because the two data had the same time step and number of data points. The results obtained are shown on chapter 5: Results and Discussion.

4. PRACTICAL ANALYSIS

In order to verify the results obtained in LTspice, two lab practices were arranged. The first meant just a first contact with the equipment and the lab environment. In the second lab practice, a monitor and a DCPS had their current and voltage waveforms analyzed for different switch phases on the power. The main purpose was to understand how and why the inrush current changes when the voltage is switched on in different phases. The original results obtained with FlukeView's software are shown below:

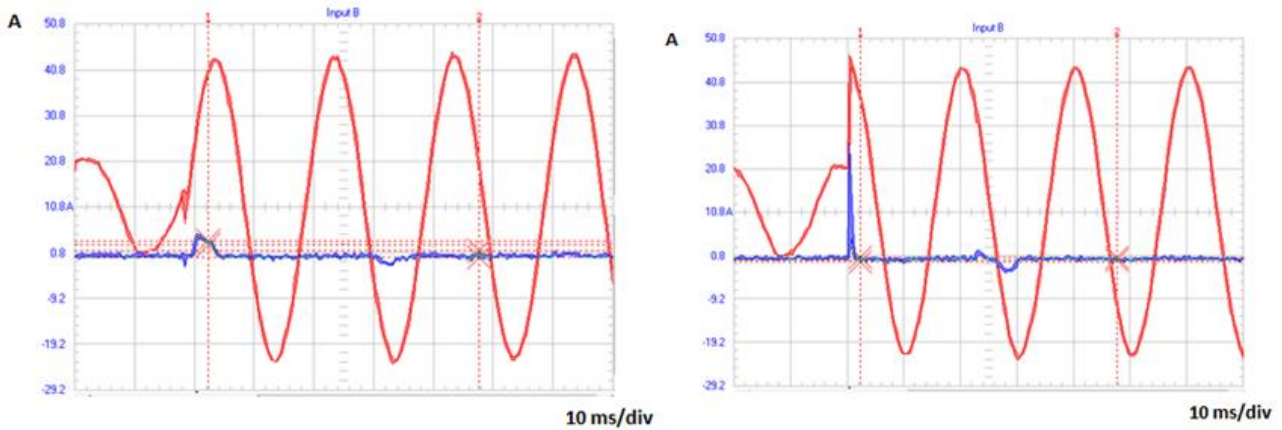


Figure 24: Monitor's waveforms when the power is switched on at 0° (on the left) and at 90° (on the right)

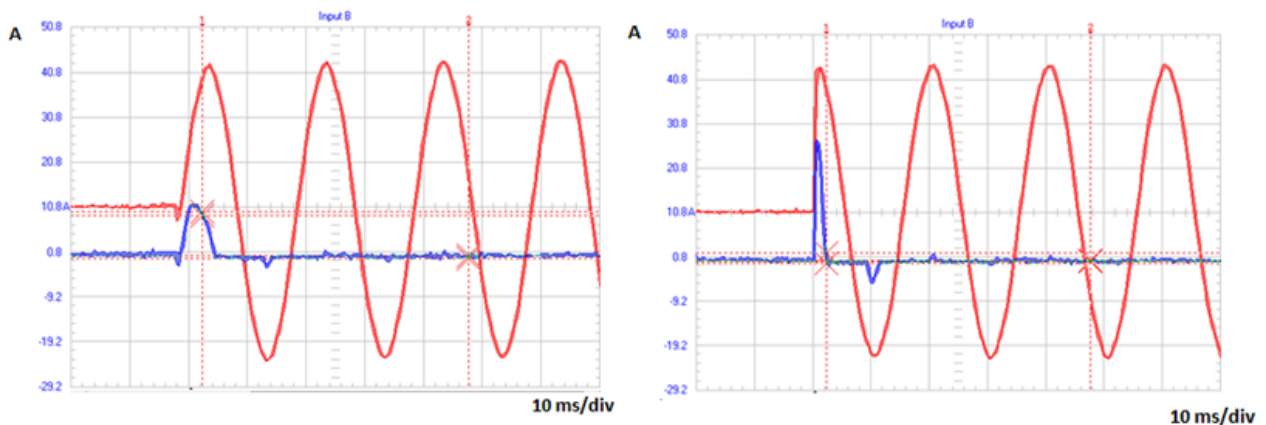


Figure 25: DCPS's waveforms when the power is switched on at 0° (on the left) and at 90° (on the right)

In the graphs, the red curve is the input voltage and the blue curve is the current on the load. By analyzing Figure 24 and Figure 25, it is possible to see that the inrush peak is the highest when the power is turned on at the peak of the voltage, which is 90° . Moreover, the current is the lowest when the voltage is turned on at the 0° . It means that to guarantee the minimum inrush current the power must be switched on in the zero-crossing, providing more

confidence to the system in medical procedures and also less changes of damaging the devices.

The measurements were also done when the power source had been switched on at 0°, 30°, 60°, 90° and also for the respective negative phases. The graphs for these mentioned phases can be found in Appendix C – Lab Measurements.

After the lab data collection, the current waveforms of the monitor and de DCPS were exported from FlukeView to Excel. A graph of the first three peaks amplitude versus the phase angle was plotted, for both loads, presenting the relation between amplitude and phase.

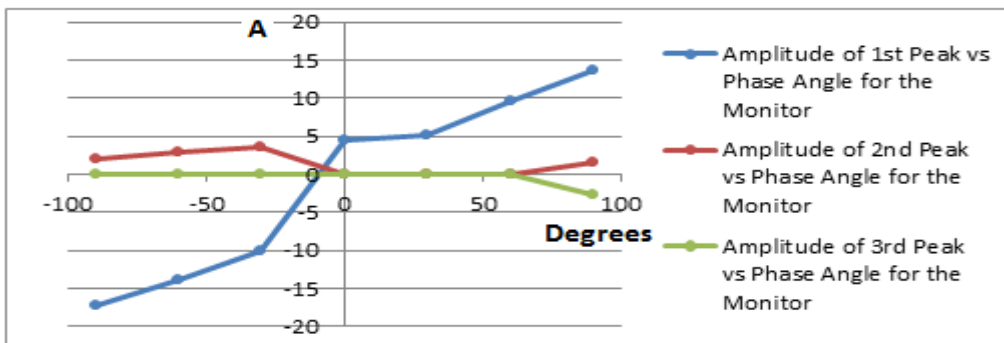


Figure 26: Current x Phase for the monitor

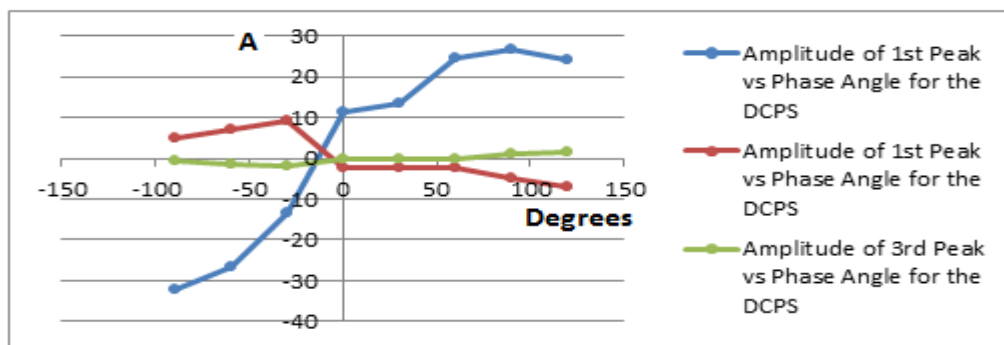


Figure 27: Current x Phase for the DCPS

The graphs show that the relation between amplitude and phase is approximately described as a sine function that is more noticeable for the first peak amplitude. The second and third peaks do not show such a significant difference in their amplitudes when changing the switch phase. Since the capacitive elements of the loads are already charged after the first peak, it is not expected that another peak of the same amplitude happens again.

After the measurements, a computational model for the monitor and for the DCPS has been developed. The circuits follow the same model shown in Figure 20. Depending on the current waveform, the resistor's function is described by one or more *if* functions. The more

complex the waveform is, more different values are attributed for the resistor and more *if* functions are needed to describe the circuit. Figure 28 and Figure 29 show the schematic for both loads.

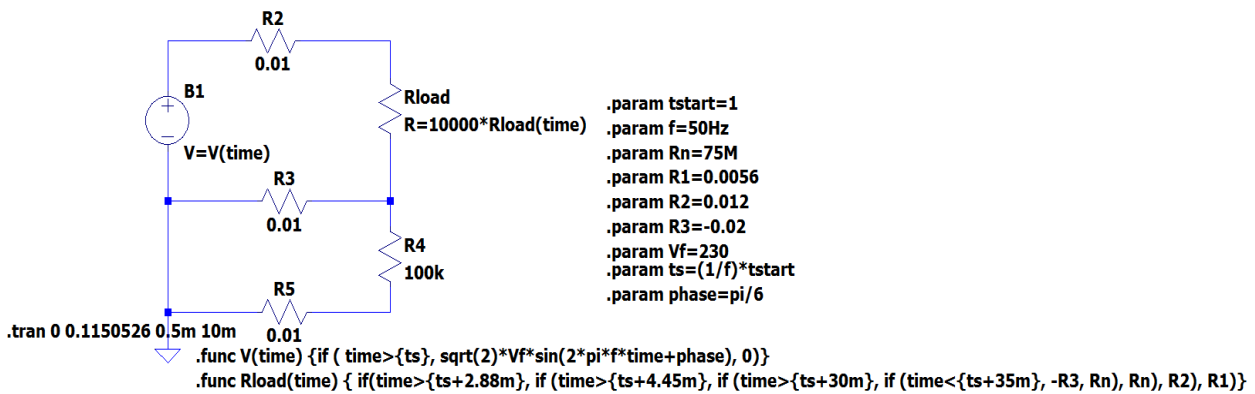


Figure 28: Monitor circuit

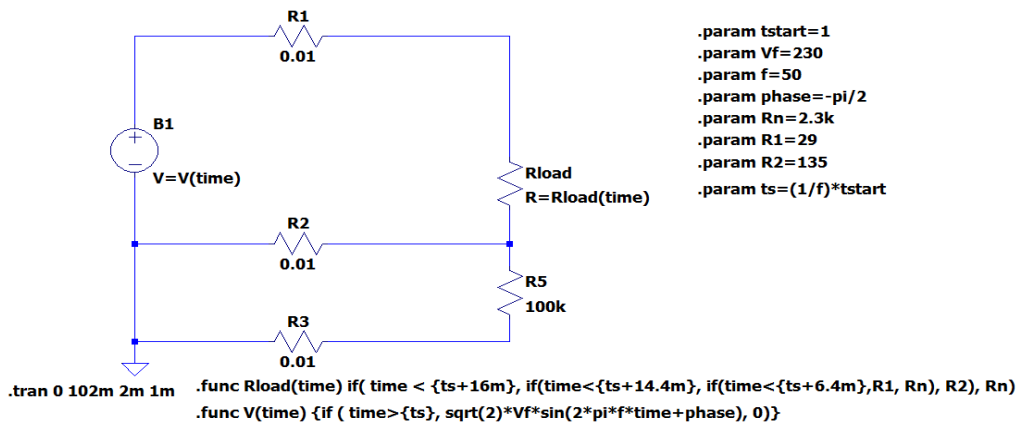


Figure 29: DCPS circuit

The two models above were built based on the current waveform generated when the voltage was switched on in the zero-crossing. The purpose of building these models is to have a circuit that, when changing the parameter *phase*, shows exactly the same current behavior as the lab measurement. However, looking at the graphs below it is possible to see that the results were not so reliable as expected.

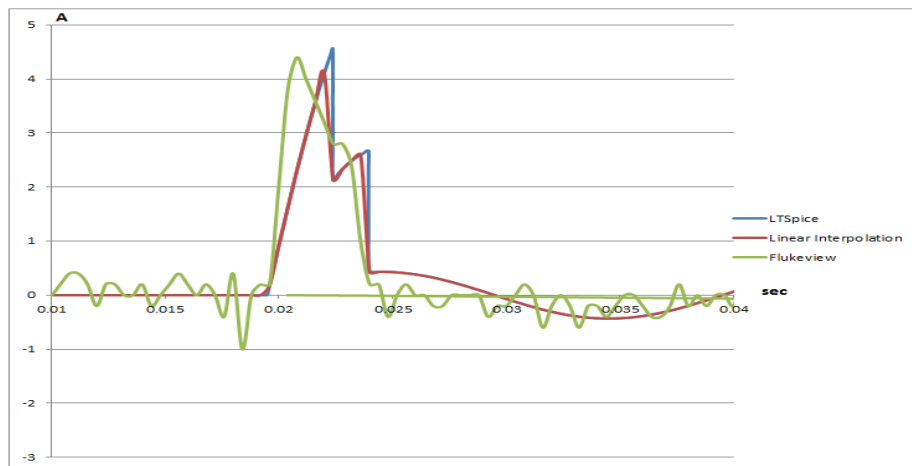


Figure 30: Validation for the monitor at 0°

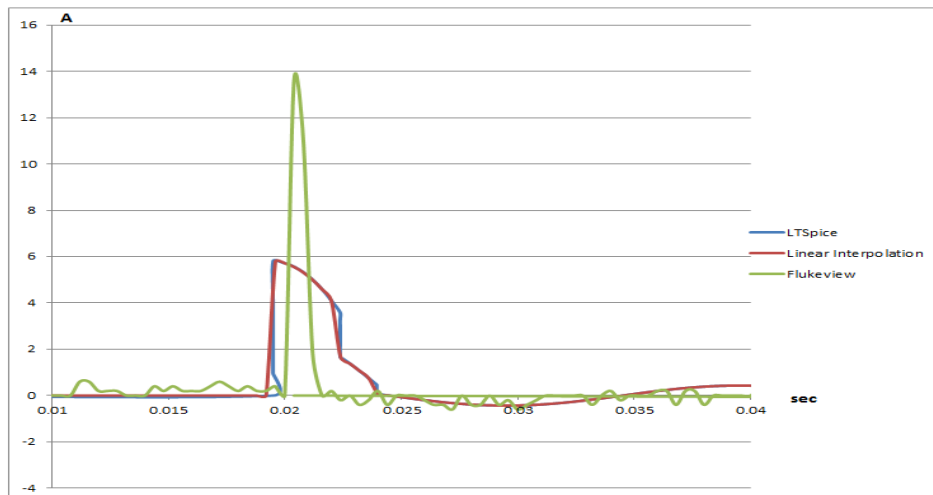


Figure 31: Validation for the monitor at 90°

For the phase 0°, it's clear the similarity between the original (FlukeView) and the computational model (LTSpice) waveforms. When the source was switched on to 90°, the similarity between the waveforms has suffered a considerable decrease. The peaks' amplitude increases when the phase is set nearby 90° and the pulse width does not follow the changes observed in the real load. As shown in Figure 31, the time duration of the peak changes, but this is not followed by the model, whose pulse width is a constant independent of the changes in phase.

The results for the DCPS are similar. For the zero-crossing they show a good similarity, but for the 90° the similarity is even lower than for the monitor.

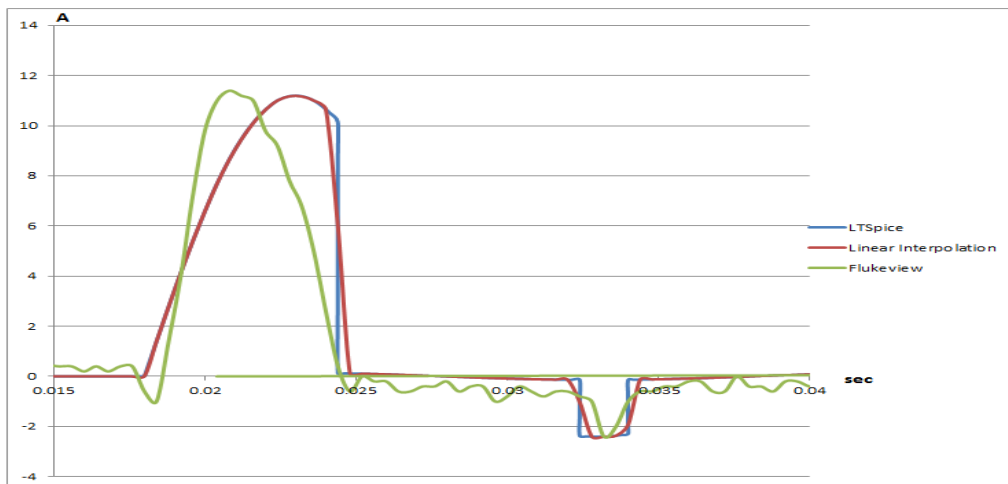


Figure 32: Validation for the DCPS at 0°

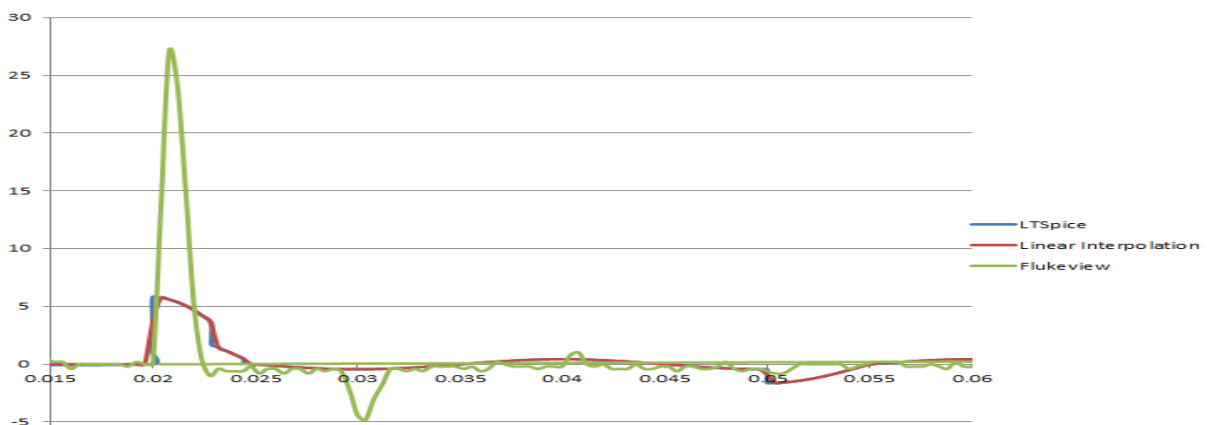


Figure 33: Validation for the DCPS at 90°

In the figure above, not only the pulse width changes, but the interval between the two peaks changes with the changing in phase as well. It's possible to see that the peaks are much closer from each other in the 90° switch than in the 0° switch. In the simulation, the distance between them keeps the same, which makes it much more different from the real load behavior and increases the error between the two curves.

The error between the interpolated data and the FlukeView curve was calculated based on the formula:

$$e = \frac{1}{n} \sum_{i=0}^n (f_i - lt_i)^2$$

where n is the number of samples, f_i is the FlukeView value of sample i and lt_i is the interpolated LTSpice value of the same sample i . The error was calculated point by point and plotted in a graph versus the time in order to have a better visualization of where the most expressive errors are.

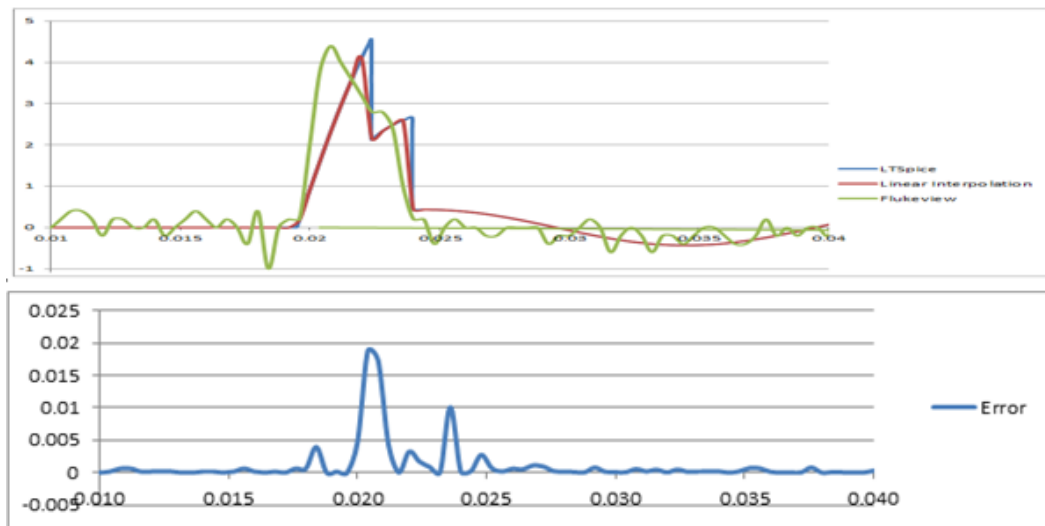


Figure 34: Error for the monitor in phase 0° .

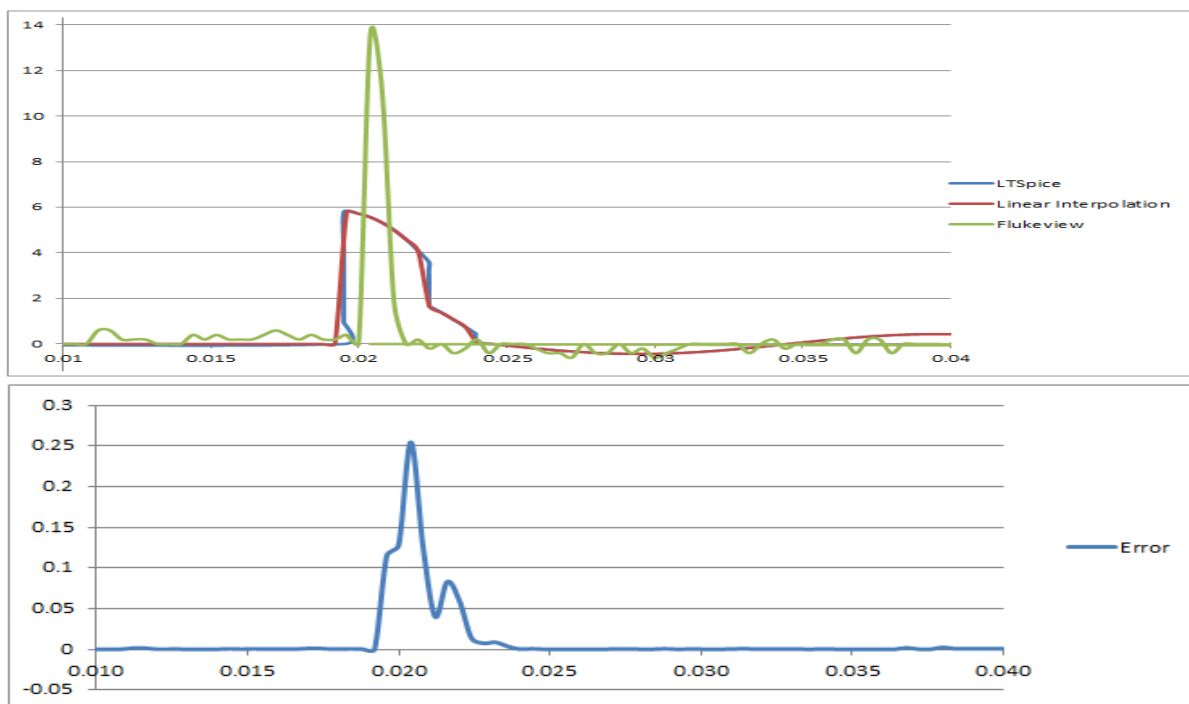


Figure 35: Error for the monitor in phase 90° .

Analyzing the graphs, it's noticeable that the higher errors occur on the peaks. This was expected, since it's difficult to simulate this variation of current exactly in the same way. Furthermore, the order of magnitude of the error changes a lot from the 0° to the 90° . In the first case, the higher error magnitude was around 0,02, whereas in the second case it was a bit more than 0,25.

For the DCPS, the following results were obtained:

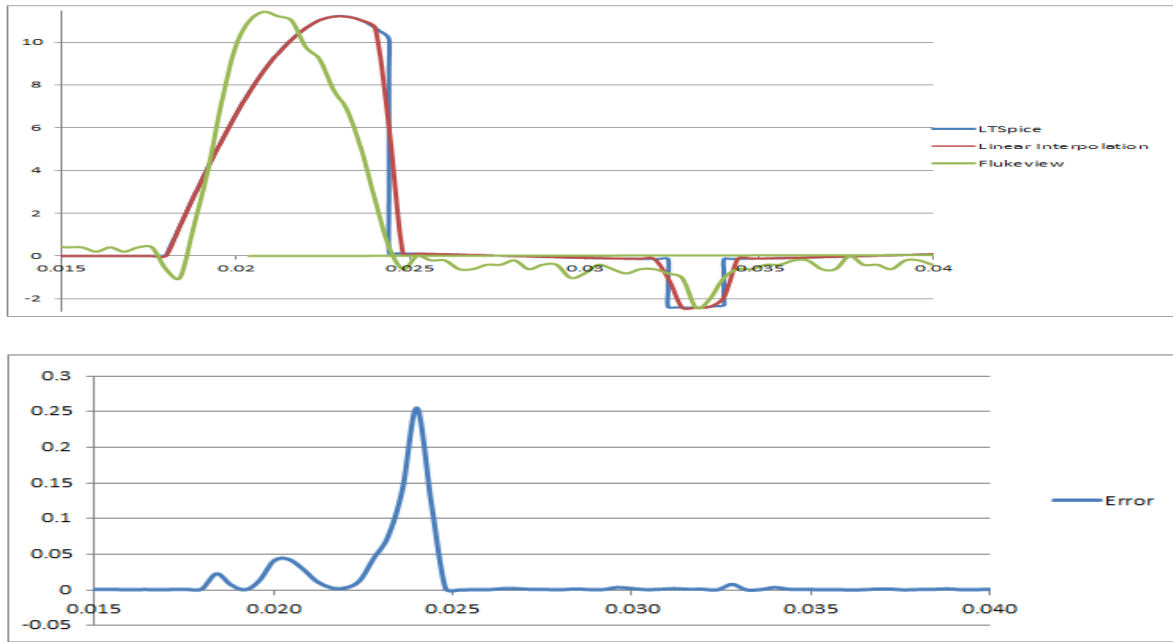


Figure 36: Error for the DCPS in phase 0°.

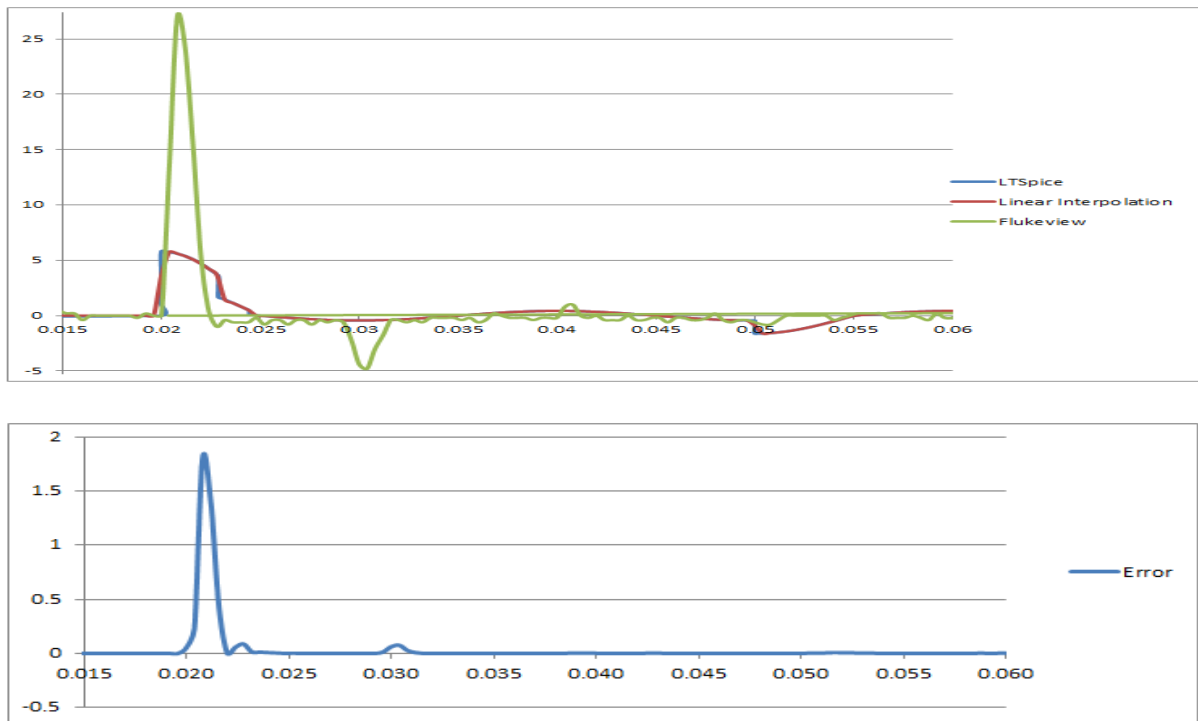


Figure 37: Error for the DCPS in phase 90°.

In this case, the DCPS LTSpice model did not represent so faithfully the real load behavior like the monitor did. Further improvements can be done in this model, in a way that both the DCPS and the monitor have their models reliable even when there are changes in

the phase. A table with the errors for all the simulated loads can be found in the next chapter, Results and Discussion.

5. RESULTS AND DISCUSSION

Considering all the graphs present in this report, two tables presenting the validation of the models were created in order to quantify the average error associated to each load. For loads of Type A to Type F, the error is presented on Table 1.

Table 1: Loads Error

TYPE	LOAD NAME	ERRO R
A	DCPS VWCB receiver modules	0.0090 57
	2nd Optical DL DVI splitter	0.0157 94
	Dual Link Splitter	0.0057 34
B	2 nd DCPS VWCB receiver modules	0.0046 46
	3 nd DCPS VWCB receiver modules	0.0069 93
C	MCS Monitor	1.3163 03
	CRCB Monitor	0.2165 05
D	16x16 DVI matrix switch	3.134
	SIB	8.0266 85
E	Host PC	40.941 55
	IP PC F	16.774 466
	IP PC L	16.562 550

F	Flexvision Dell PC	0.0436 5
	Tube Cooler F	30.667 845
	Tube Cooler L	7.5102 07

Analyzing Table 1, it is remarkable that, in general, the created models have a high level of similarity presenting an error smaller than 10. However, in loads from type E, except for the Dell PC, the error is larger than the expected. Loads from this type are basically composed by two peaks, one in the negative and one in the positive Y axis area. When these curves are represented in LTspice, the peaks from the original and from the created load do not match exactly because the LTspice curve tends to follow the voltage waveform. This is something undesirable, because the shape of the inrush peak sometimes is really steep and short, whereas in the simulation it's only possible to have an inrush peak that looks like a sine wave.

In the case of the Tube Cooler F, the high magnitude of the error can be explained based on the fact that there is a shifting between the waveform provided by FlukeView and the one provided by LTspice interpolation. Although there is a good matchup between the mentioned waveforms when the graphs are visually analyzed, the magnitude of the average error is surprisingly big. It might be that due to this shifting, the points analyzed for the interpolation are not in the same time in FlukeView, causing also some shifting in the error plot.

Table 2 presents the average error of the monitor and the DCPS analyzed in the Lab. As already mentioned, all the loads were created based on a zero phase switch-on. This way, when the switch-on happens in a different phase, the model presented some unexpected behavior and some differences when comparing to the original waveform. By analyzing this table, it looks like when the phase is changed the results are reasonable, but looking at the plots, the curves does not matchup so well. Surprisingly, in both models the error of some non-zero phases is even smaller than in the zero phase. All these facts shows that the method used for the error calculation might not be the most appropriate for this validation.

According to statistics definitions, the average error is one of many ways to quantify the difference between values implied by an estimator and the true values of the quantity being estimated. Unfortunately, the use of this method suppresses the most expressive errors, giving some kind of wrong impression about the model behavior. [7]

Table 2– Monitor and DCPS Errors

LOAD	ERROR						
	0°	30°	60°	90°	–30°	–60°	–90°
Monitor	0.180778	0.001128	0.002449	1.087465	1.04612	0.003399	1.480049
DCPS	0.0037 75	1.519 495	0.015 159	0.017 271	0.00 799	0.028 657	0.022 769

Considering the analyses of both tables and of the all graphs present in this report, it can be said that the models are a nice representation of the corresponding original one, offering a quick and easy way of observing some complex kind of loads when the source is switched on at zero phase and different phases. Although the results present in these tables are reasonable, the error calculation method could be improved in the future in order to increase the quality of the building models.

6. CONCLUSIONS

The aim of this assignment was the development of computational models capable of offering reliable results in a short period of time and that provide the analysis of the inrush behavior associated to loads that take part in a medical room. During the model creation's period, many ideas came up in order to generate the required current waveform in a circuit composed only by resistors, capacitors and inductors. But also with the ideas, a lot of troubles and difficulties emerged until the best model was chosen. In parallel with the load model development, a magnetic simulation, also in LTspice, was created in order to analyze how magnetic components behave under the core saturation.

After some non-efficient methods to obtain the required inrush behavior, it was decided to describe a resistor using *if* functions in order to obtain the closest pulse width and current peak amplitude to the original as possible. Since that, all the loads were divided in six different types that present the same characteristics and could be defined using the same *if* function structure, changing only values related to the time and amplitude parameters. By using this method, the results obtained for the loads were, by looking, really satisfying, but it became necessary to validate these models and see if the relation with the original waveforms was as good as expected.

In order to validate all the results, it became necessary to interpolate the points that came from LTspice with the aim of reaching the same sampling numbers and time step that comes from FlukeView. Once interpolated, the average error between the waveforms could be calculated.

Tables 1 and 2 present the error found for all the building loads. As already discussed, it is remarkable that, in general, the created models have a high level of similarity, most of them presenting an error smaller than 10. Though the tables present such good results, some loads still need improvements and the error calculation method is still not the most efficient, since the use of the average error method is not really expressive when an analysis of the error in a determinate period of time is required.

In conclusion, considering all the results obtained, it can be said that the models created in LTspice are a very good way to simulate and represent real life loads in a medical room. A good recommendation to the next group that will take place in this project is to look for different ways to calculate these errors, improving the loads that are not so accurate. Moreover, further improvements have to be done in the magnetic components simulation, in order to obtain a model that represents low-frequency hysteresis. And finally, it's necessary

to make some changes in the computational model, making it compatible with the real load behavior even when the user changes the switch-on phase.

APPENDIX A – LOAD MODELING

In order to visualize one of the most expressive behaviors of the load, the inrush current, a few techniques to vary the impedance of the computational load model were applied. In the beginning, a single load was designed using first a variable resistor. In this case, a resistor was set to have its value increased during the same period of time. The initial value was set and increased by a defined increment until it reaches a predetermined final value. The circuit analyzed using this variable resistor is illustrated in Figure 38.

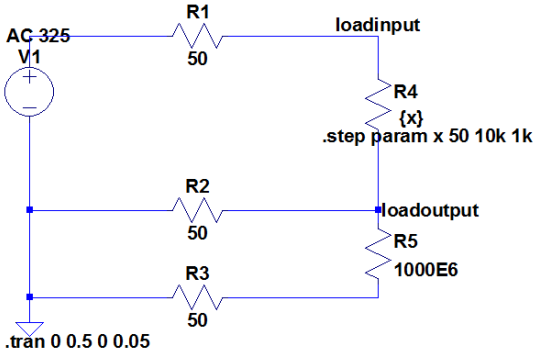


Figure 38: A single phase source with a variable resistor

The waveforms for voltage and current on the load are illustrated in Figure 39.

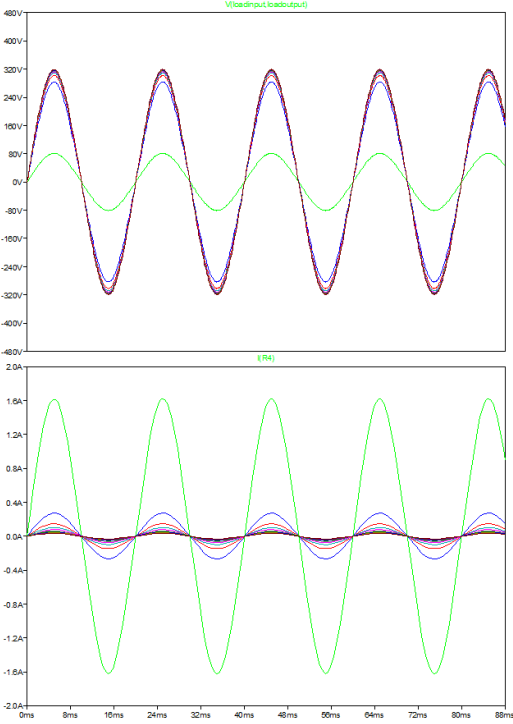


Figure 39: Output voltage and current on the resistor

The inrush current could not be visualized in this model, so it was necessary to choose another way to represent the load. The second step taken was based on a varistor. A varistor is an electronic component with a nonlinear current–voltage characteristic, similar to a diode. This kind of component is often used to protect circuits against excessive transient voltages by incorporating them into the circuit in such a way that, when triggered, it will shunt the current created by the high voltage away from sensitive components. The schematic is illustrated in Figure 40. [8]

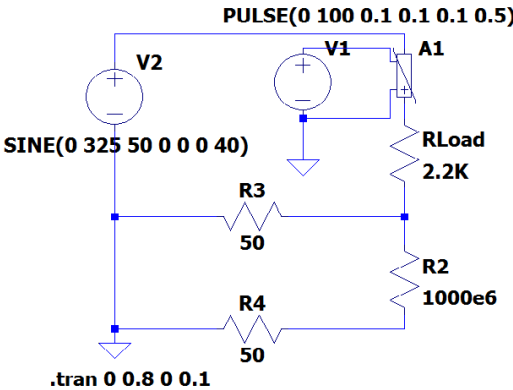


Figure 40: A single phase source with a varistor

The voltage waveforms on the voltage source, on the varistor terminals and on the load, as well as the current waveforms on the voltage source and the on the load are presented in Figure 41.

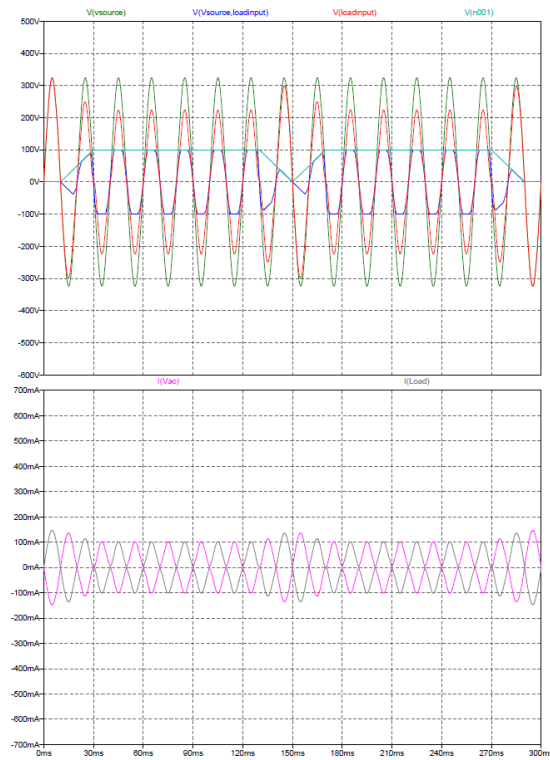


Figure 41: Output voltage and current on the varistor

By analyzing the figure above, the inrush current still could not be observed, only a decrease on the current amplitude when the varistor is triggered. After testing both techniques mentioned, a resistor was described as a mathematical function that could clearly describe the inrush current and the current damping during the time. This resistor model was already presented in “Software Simulation” in the Load Model Building section.

APPENDIX B – LOAD TYPES

The complete description of the load types is shown below.

✓ Type A

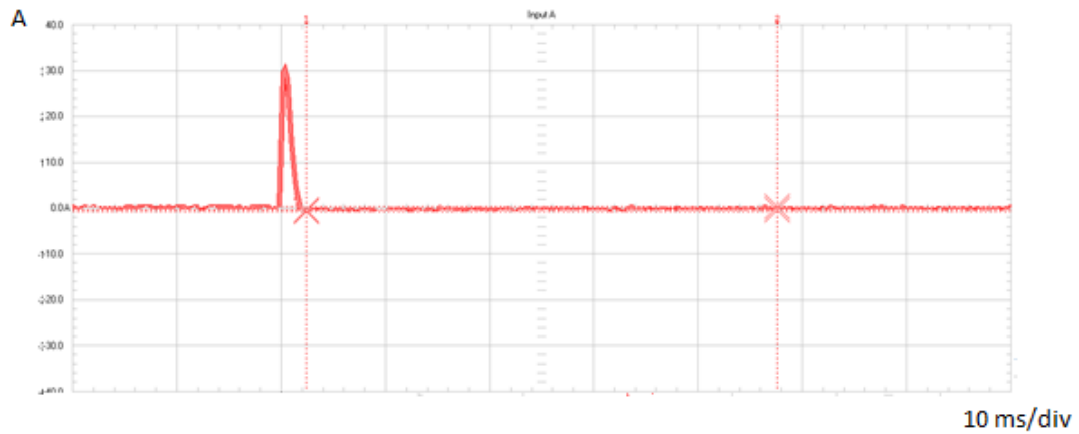


Figure 42: 1st DCPS VWCB receiver modules (B-Cabinet)

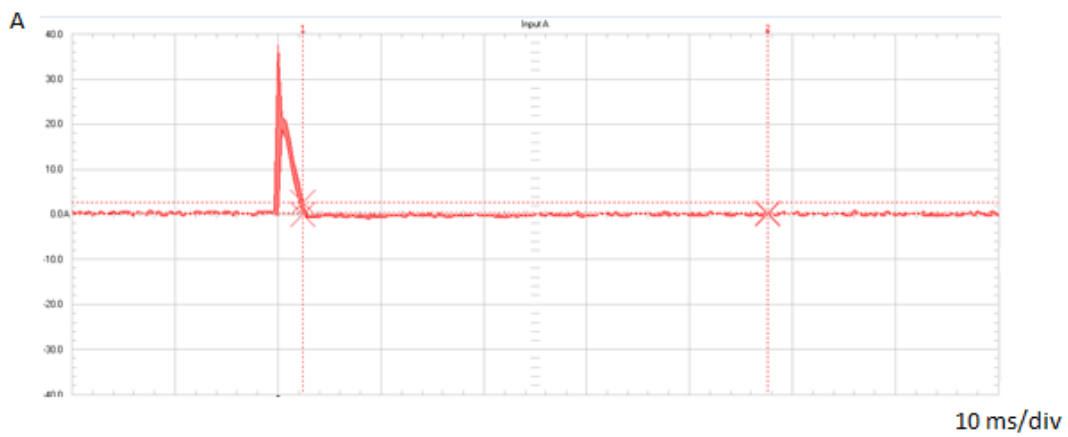


Figure 43: 2nd Optical DL DVI splitter (B-Cabinet)

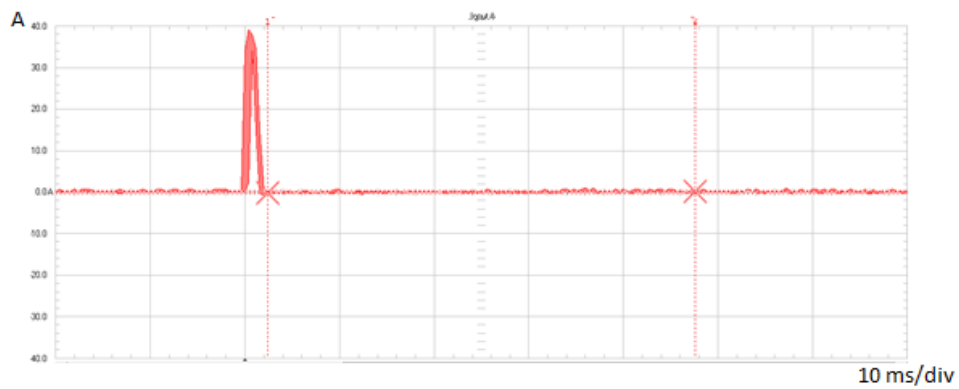


Figure 44: Dual Link splitter (B-Cabinet)

✓ Type B

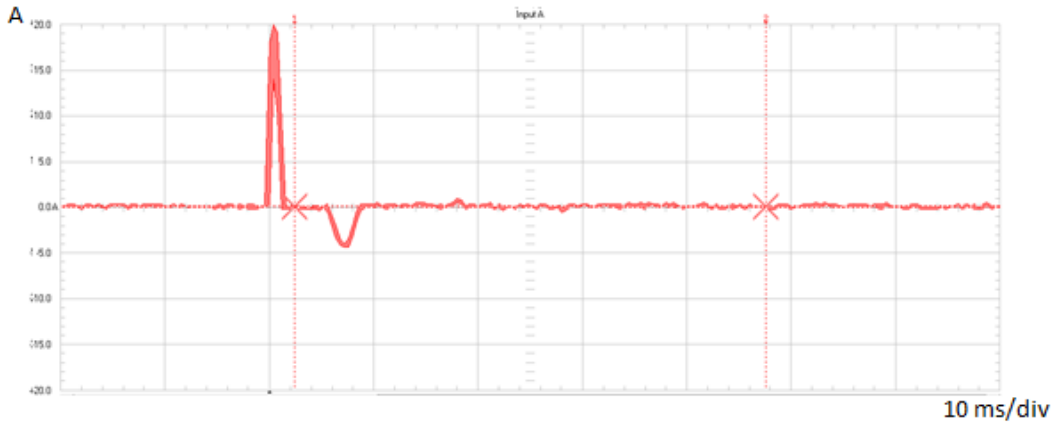


Figure 45: 2nd DCPS VWCB receiver modules (B-Cabinet)

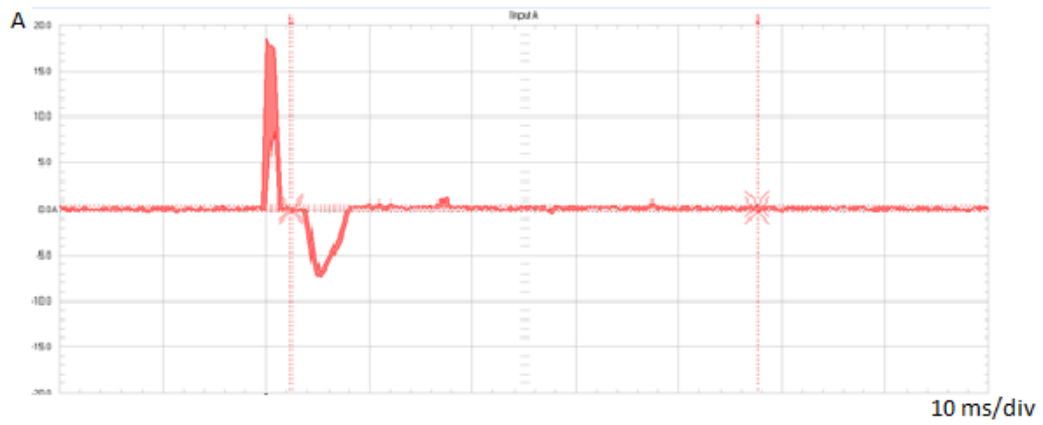


Figure 46: 3rd DCPS VWCB receiver modules (B-Cabinet)

✓ Type C

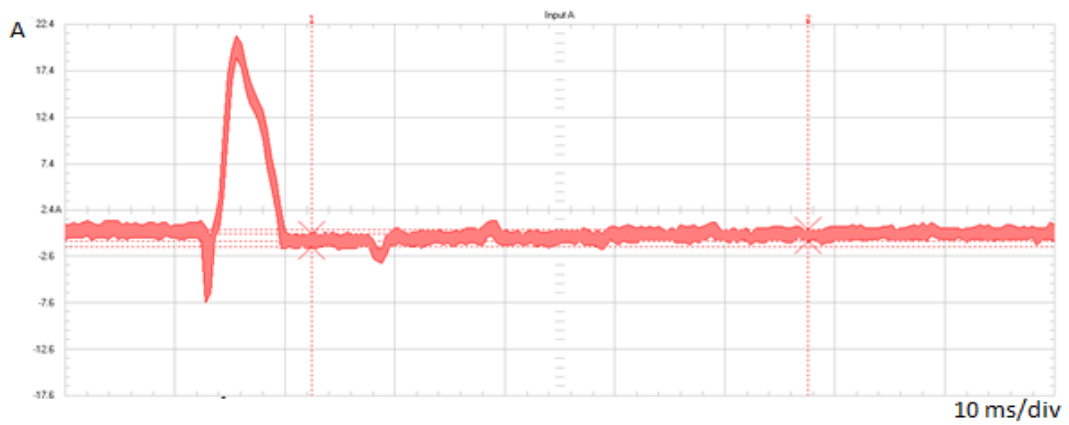


Figure 47: 2nd MCS monitors (WME 1.8) (M-Cabinet)

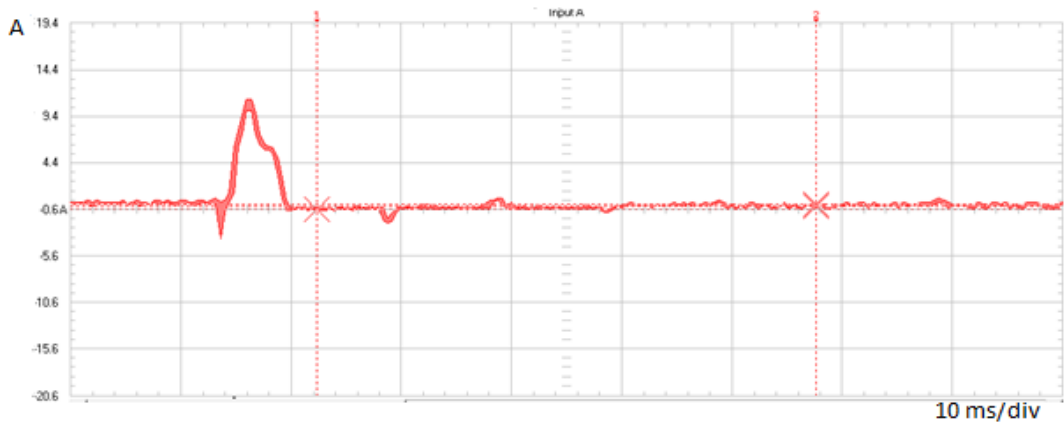


Figure 48: CRCB continuous (M-Cabinet)

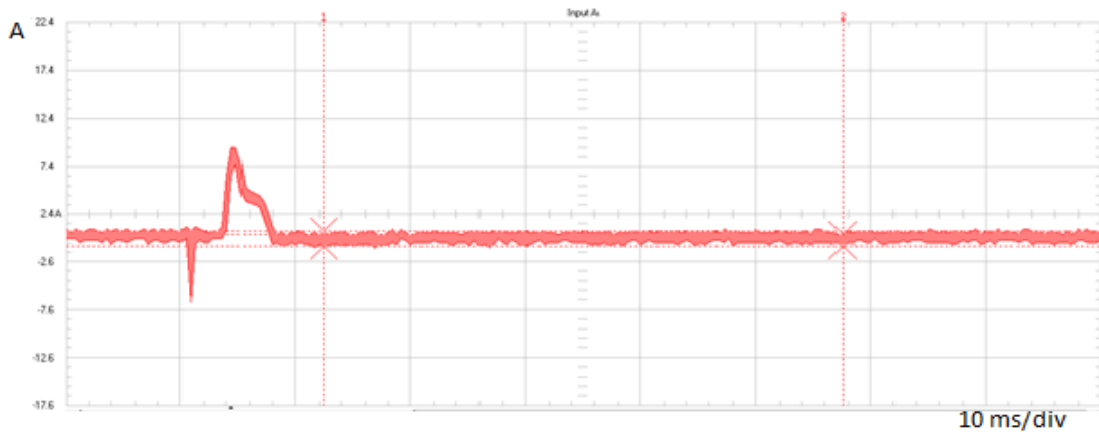


Figure 49: CRCB switched (M-cabinet)

✓ Type D

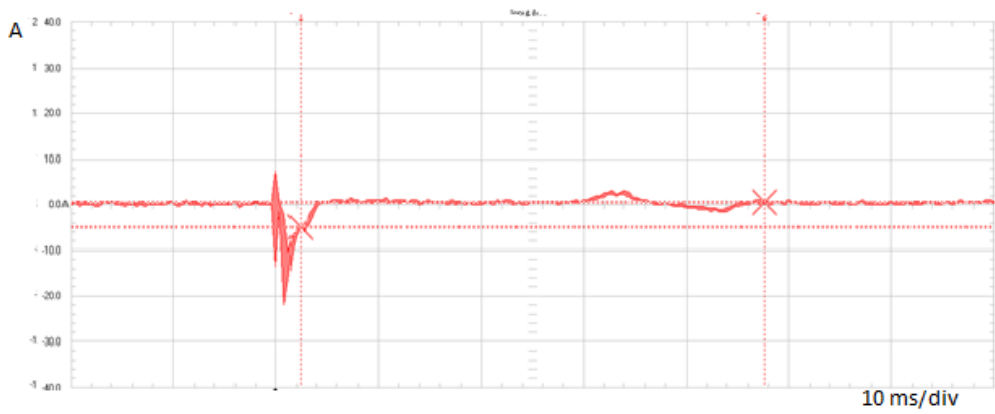


Figure 50: 16x16 DVI matrix switch (B-cabinet)

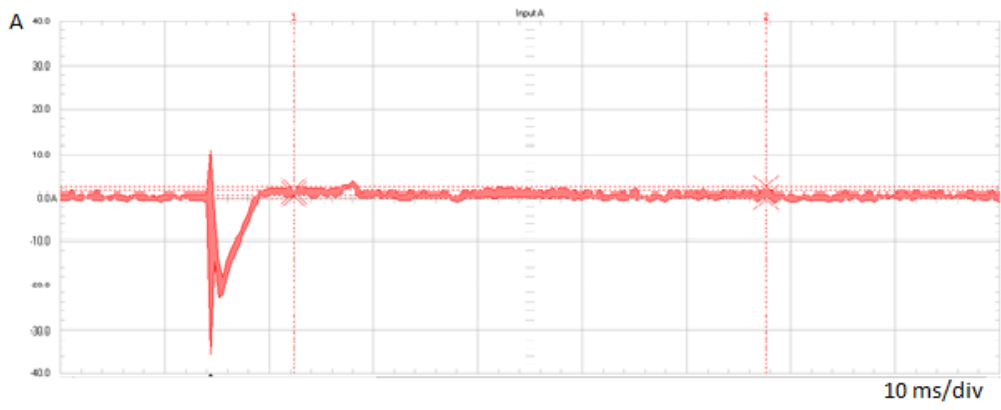


Figure 51: SIB (M-cabinet)

✓ Type E

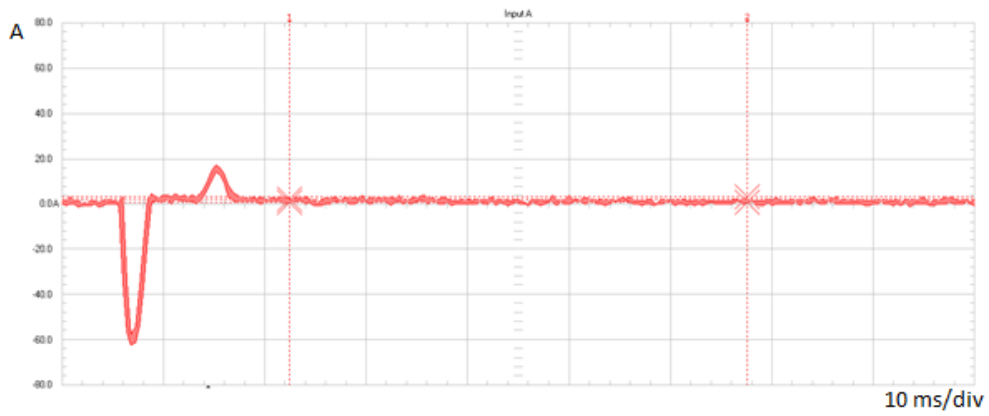


Figure 52: Host PC (M-Cabinet)

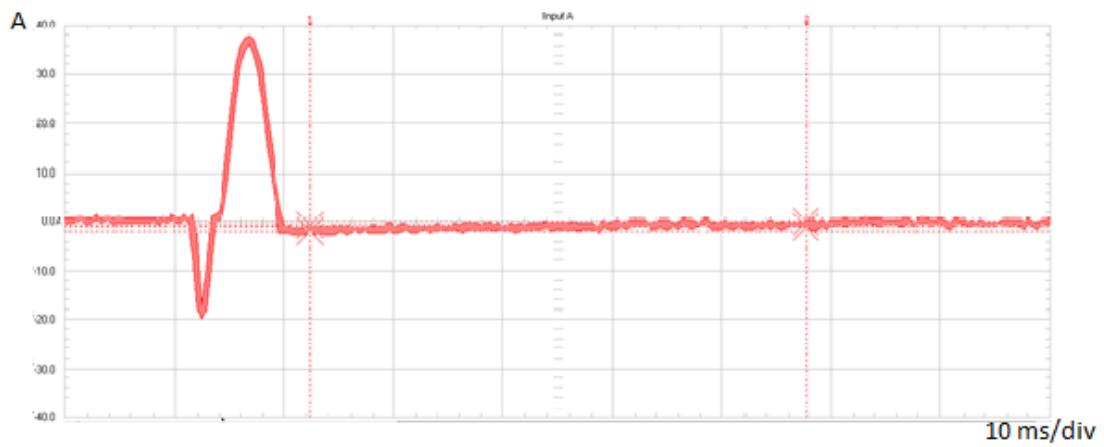


Figure 53: IP PC F (M-Cabinet)

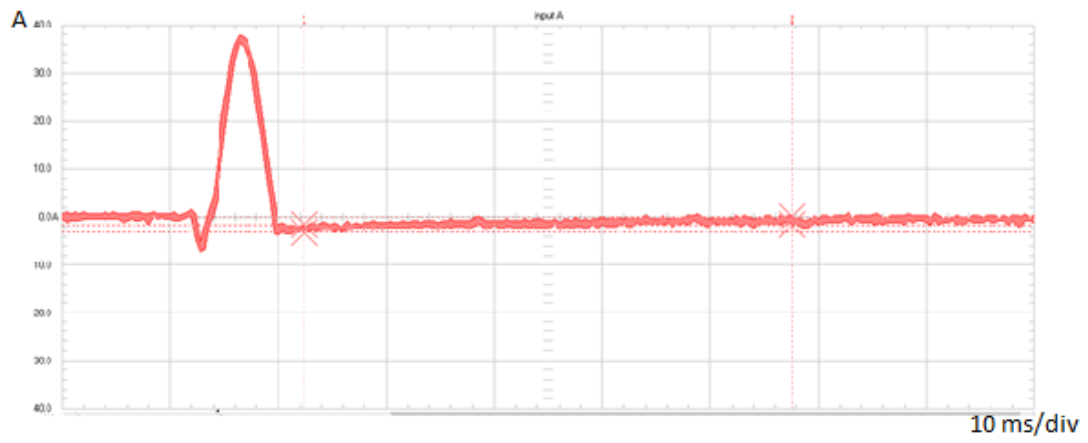


Figure 54: IP PC L (M-Cabinet)

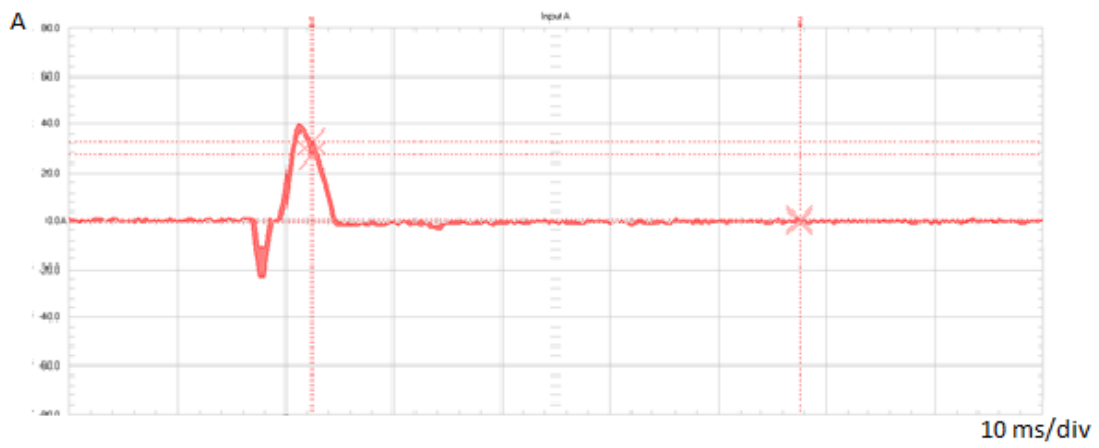


Figure 55: Flexvision Dell PC (B-cabinet)

✓ Type F

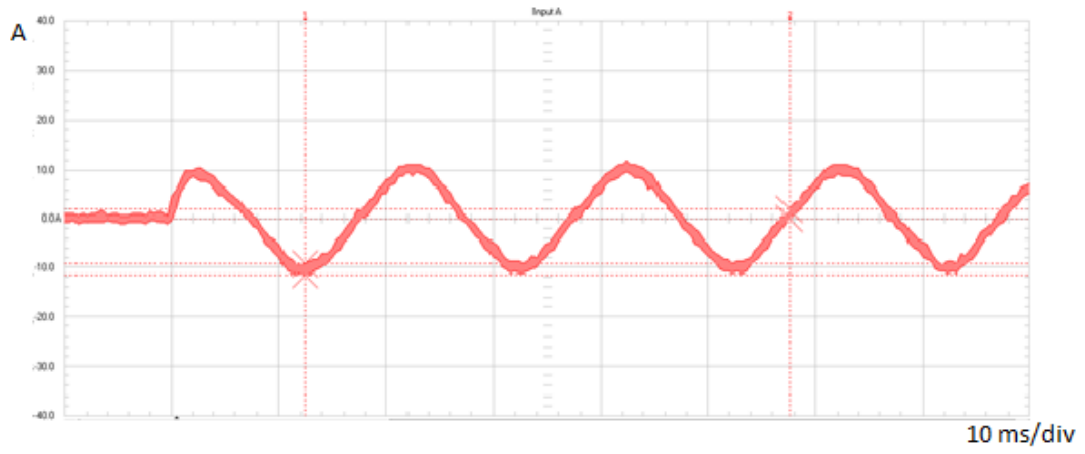


Figure 56: Tube Cooler F (M-Cabinet)

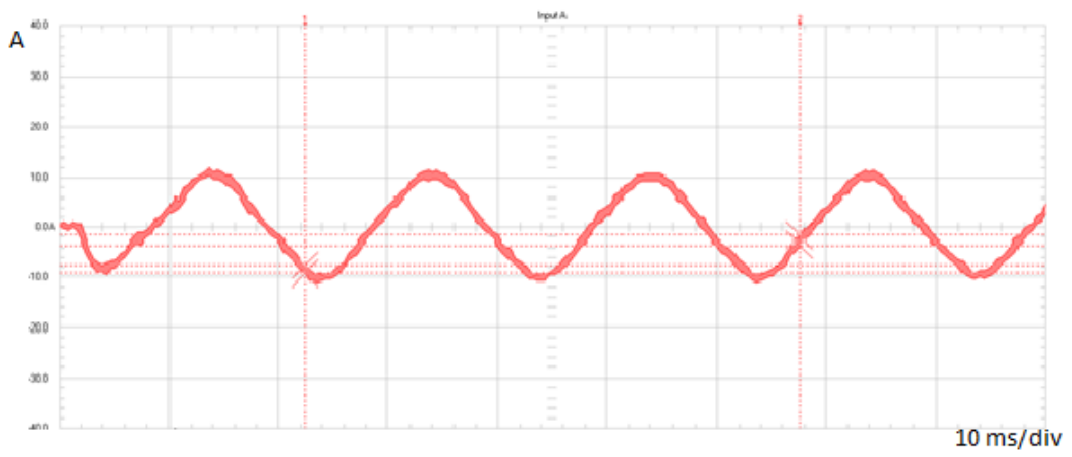


Figure 57: Tube Cooler L (M-Cabinet)

APPENDIX C – COMPUTATIONAL MODEL

The graphs below are composed by four waveforms: the data import from the scopemeter (FlukeView), the data import from the model created in LTspice, the interpolation of LTspice data and the error between the FlukeView curve and the interpolated curve.

In all of the graphs present in this appendix, the X axis represents the time in seconds, the primary Y axis (on the left) represents the amplitude in Amperes, while the secondary Y axis (on the right) represents the amplitude of the error.

✓ Type A

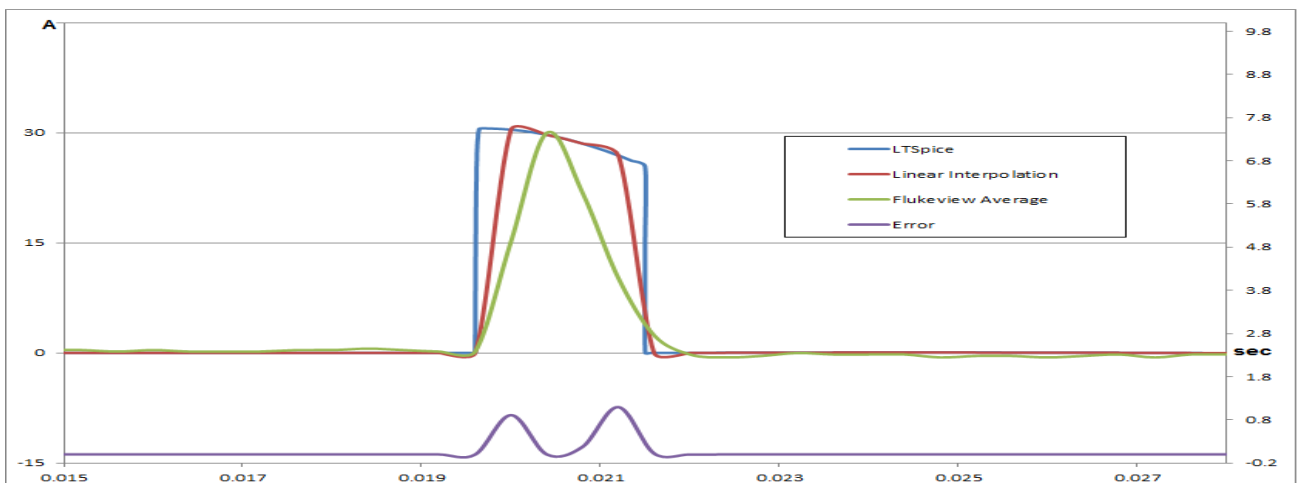


Figure 58: 1st DCPS VWCB receiver modules

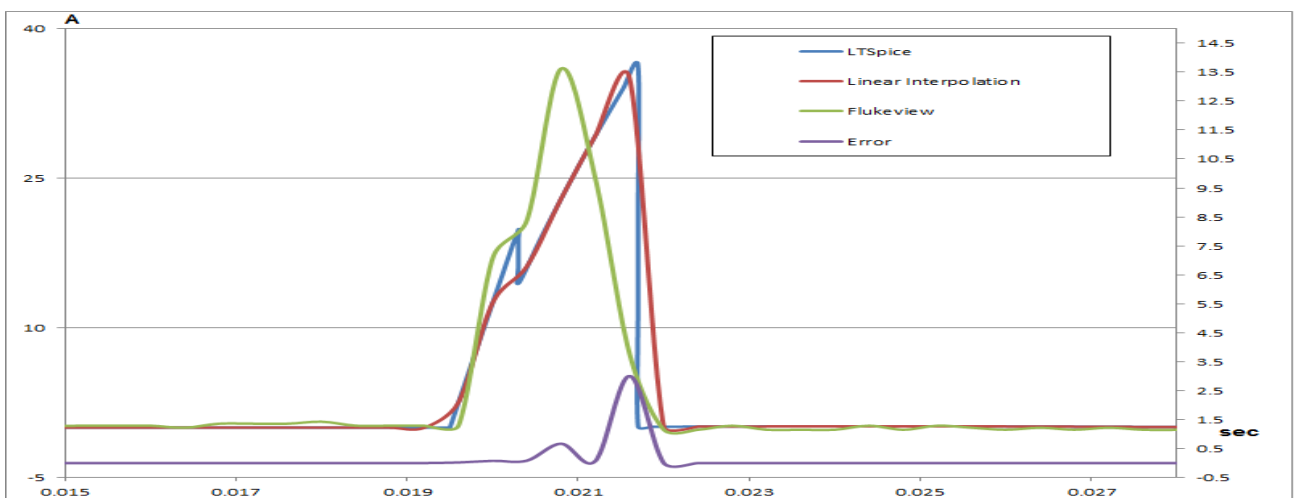


Figure 59: 2nd Optical DL DVI splitter

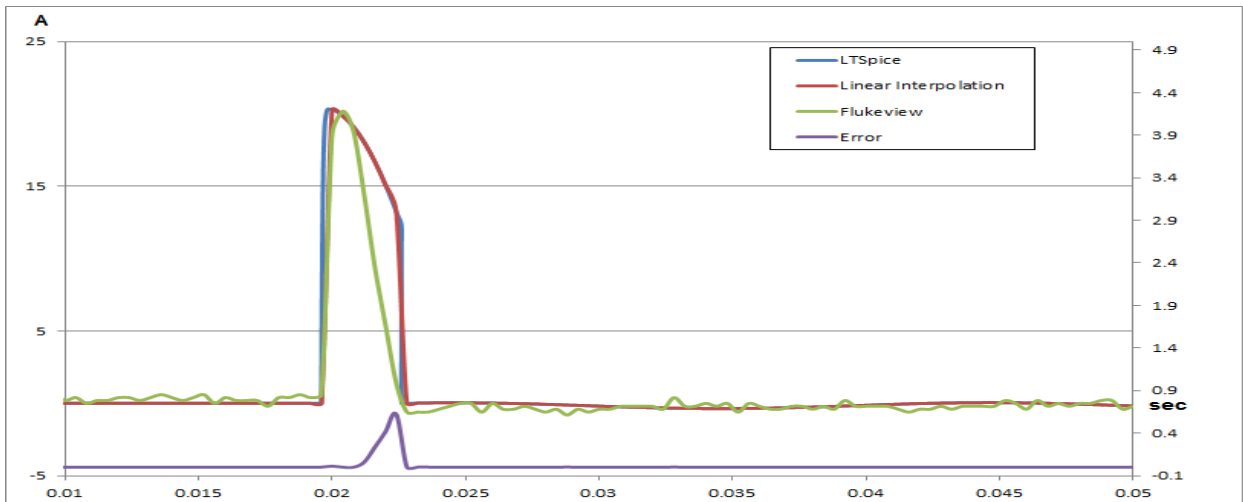


Figure 60: Dual Link Splitter

✓ Type B

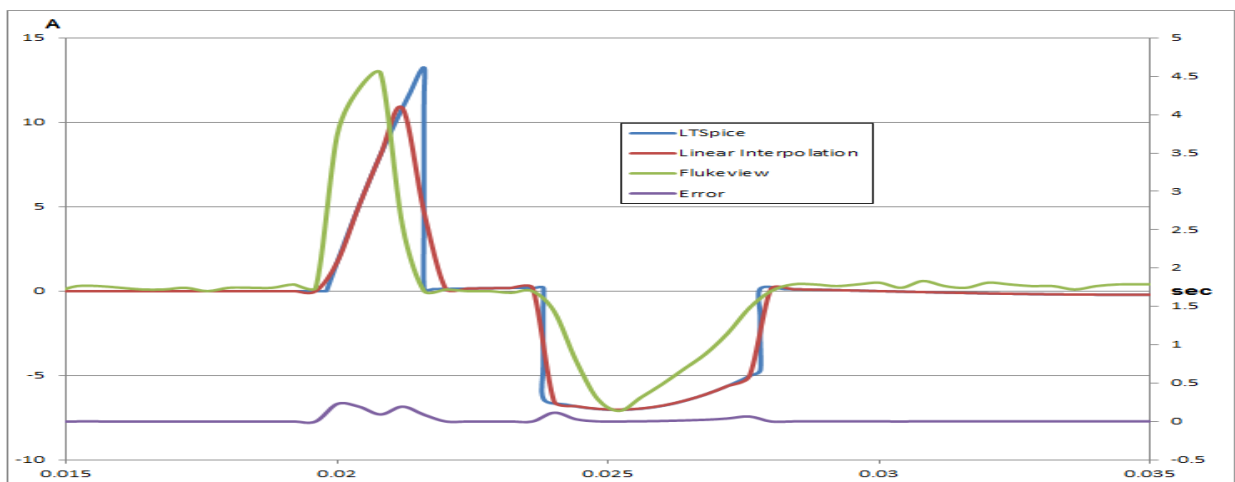


Figure 61: 2nd DCPS VWCB receiver modules.

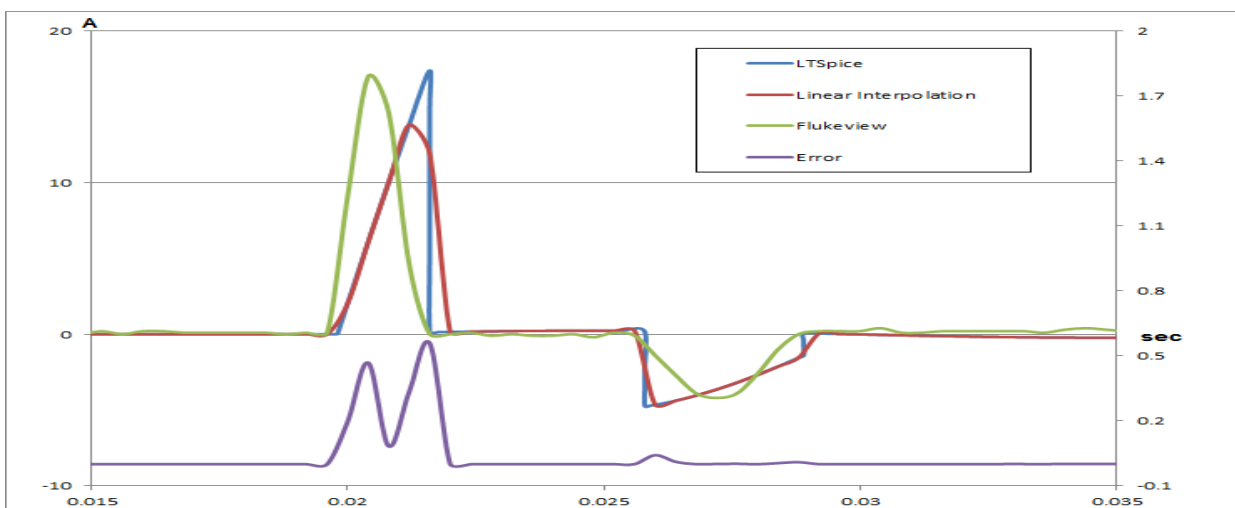


Figure 62: 3rd DCPS VWCB receiver modules

In loads of Type A and B, a capacitor was included in series with the resistor. This was necessary because without an active component, the resulting current of a pure resistive load has the shape of a sine wave, whereas the real inrush behavior presents a shorter and steeper pulse width. Therefore, in all of the DCPS loads, capacitors of 600 μ F and 300 μ F were added to the circuit and also in the 2nd Optical Dual DVI Splitter (a capacitor of 7mF) and in the Dual Link Splitter (200 μ F).

✓ Type C

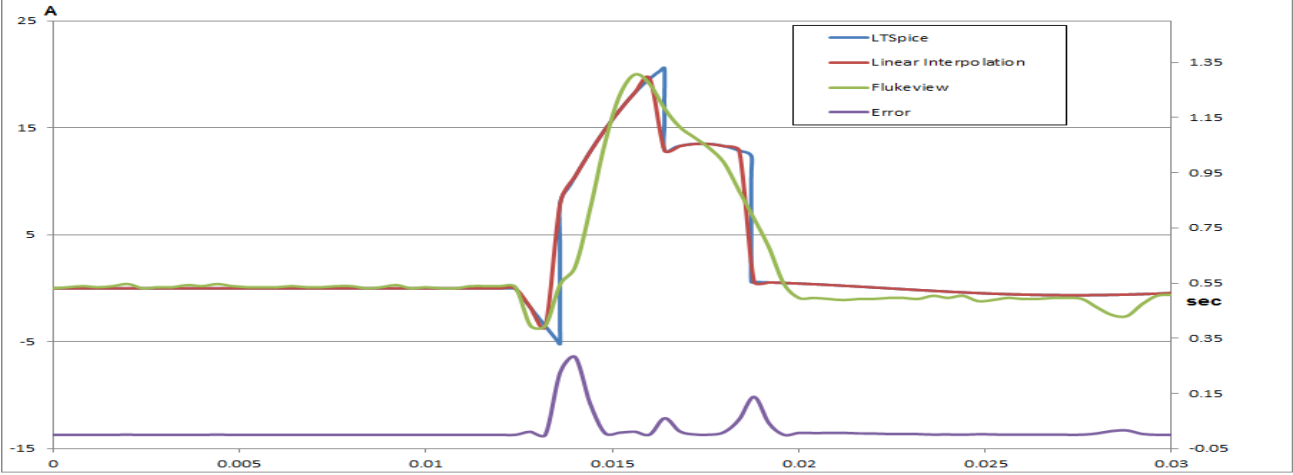


Figure 63: MCS Monitor

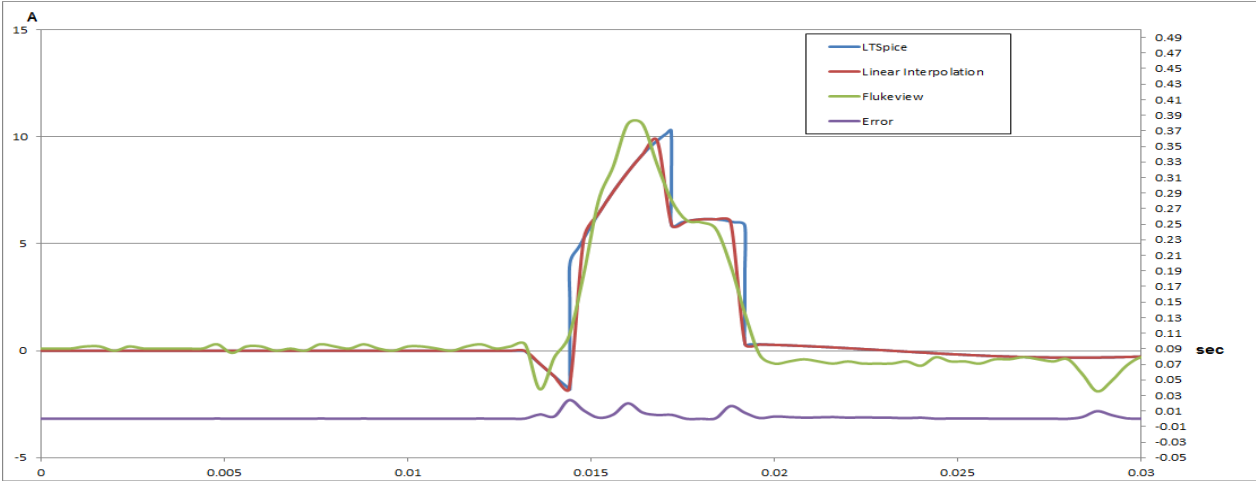


Figure 64: CRCB Monitor

✓ Type D

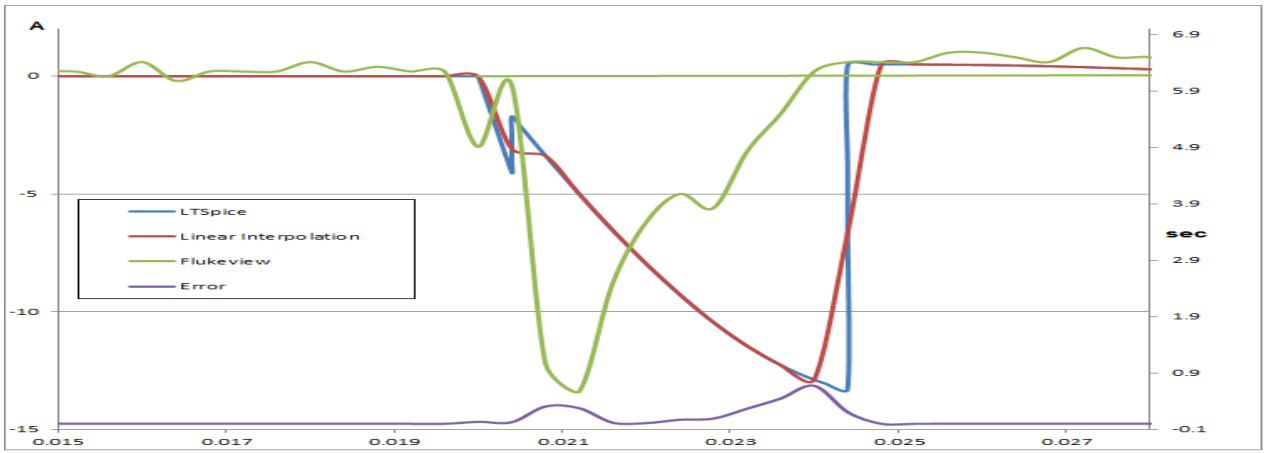


Figure 65: 16x16 DVI matrix switch

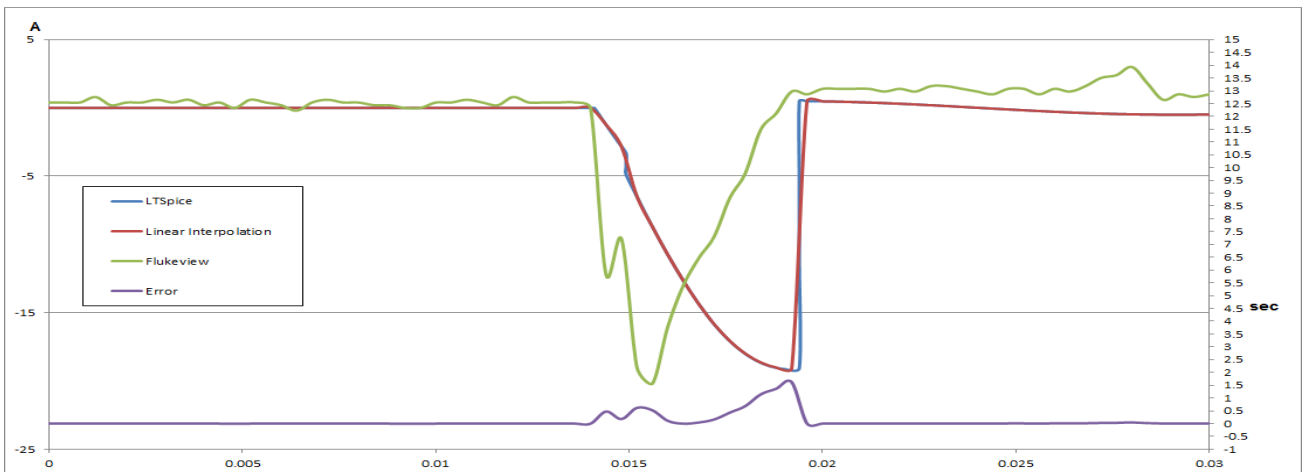


Figure 66: SIB

✓ Type E



Figure 67: Host PC

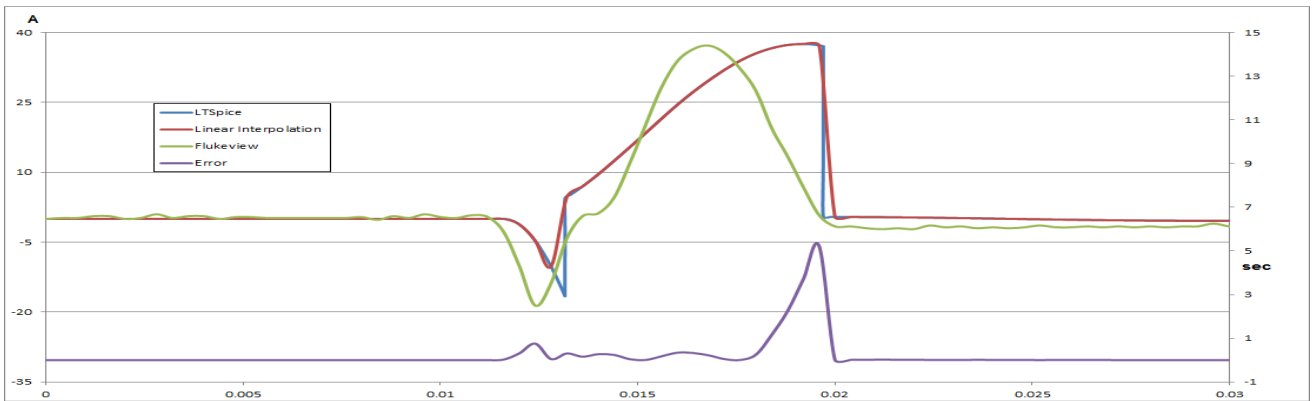


Figure 68: IP PC F

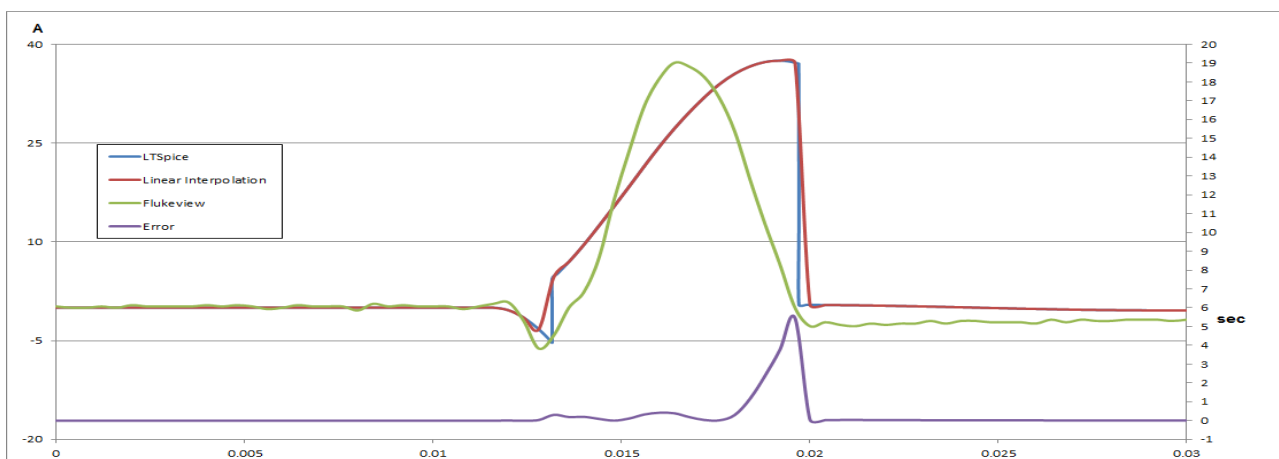


Figure 69: IP PC L

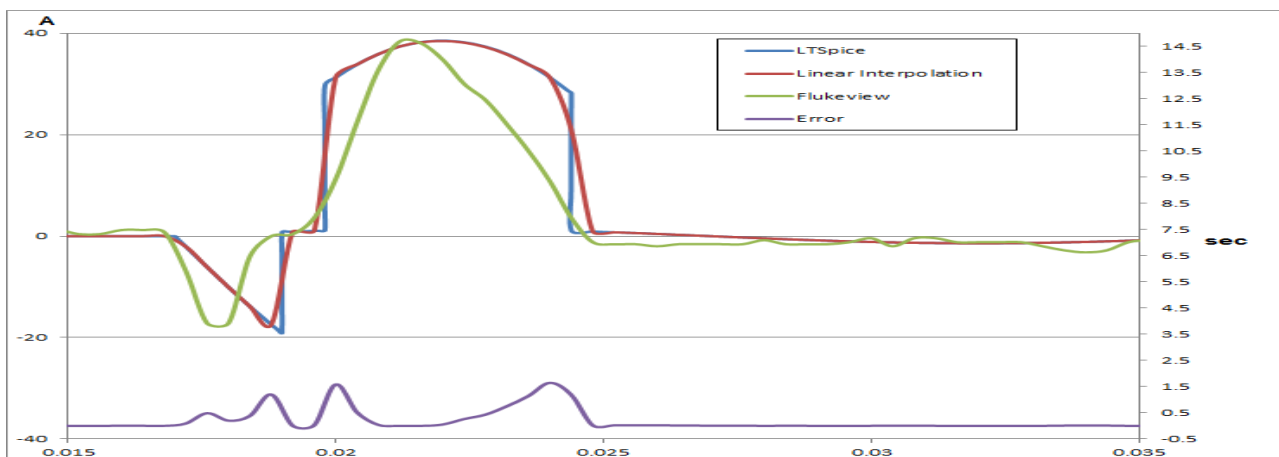


Figure 70: Flexvision Dell PC

In the schematics that represents the IP PC F and the IP PC L, one capacitor of $200mF$ was included in parallel with the resistor. This way, the peak in the positive area of the graph could be thinner, fitting in a better way the original waveform.

✓ Type F

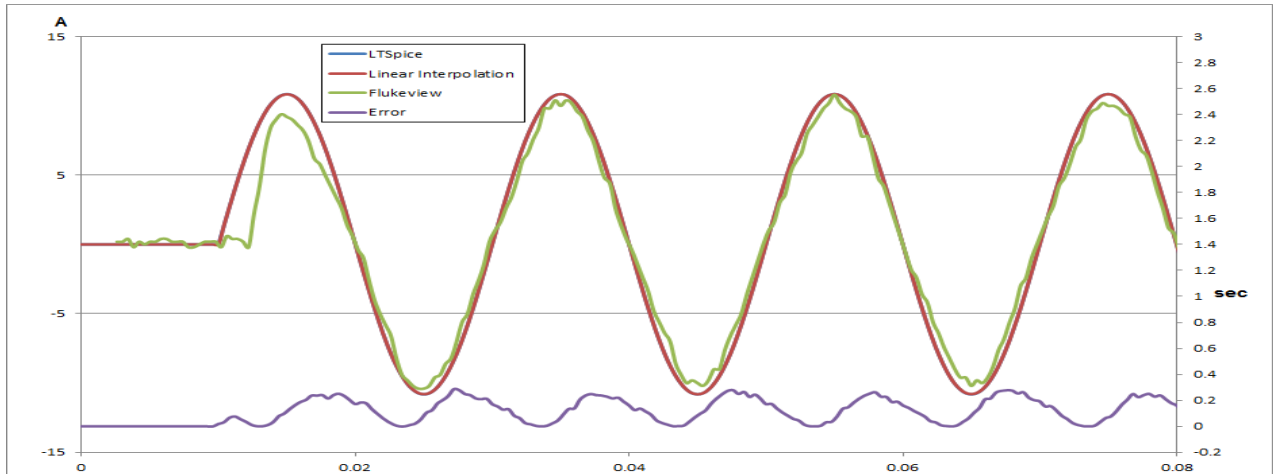


Figure 71: Tube Cooler F

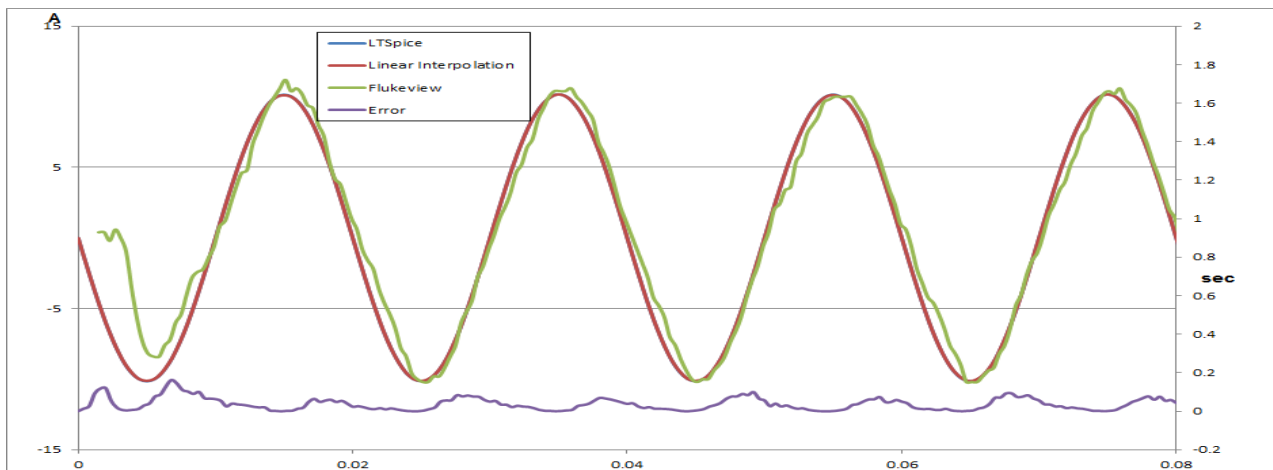


Figure 72: Tube Cooler L

In the Figures 71 and 72 above, the interpolation process did not cause many distortions in the waveform. This way, most of the curves before and after the interpolation are overlaid. Furthermore, the error curves are smaller because the current waveforms were prioritized.

APPENDIX D – LAB MEASUREMENTS

The complete waveforms obtained in the Lab, for the monitor and for DC Power Supply (DCPS), are present below. In the figures, the red curve is the input voltage and the blue curve is the current in the load.

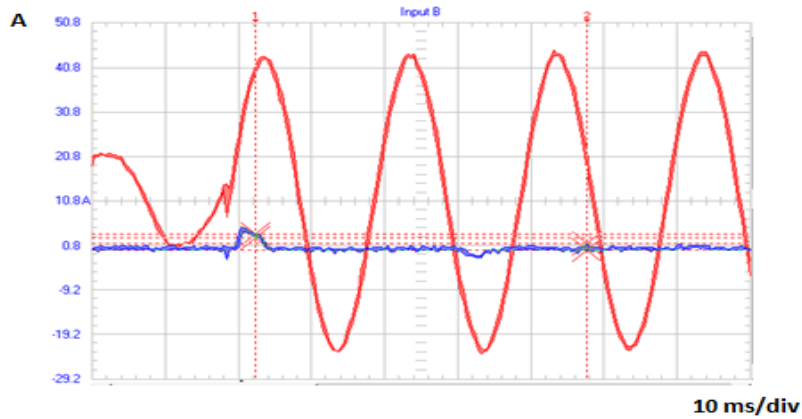


Figure 73: Monitor (power switched in phase 0°)

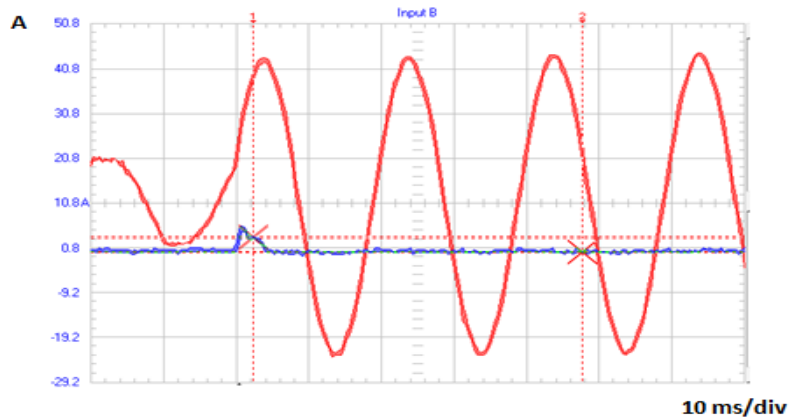


Figure 74: Monitor (power switched in phase 30°)

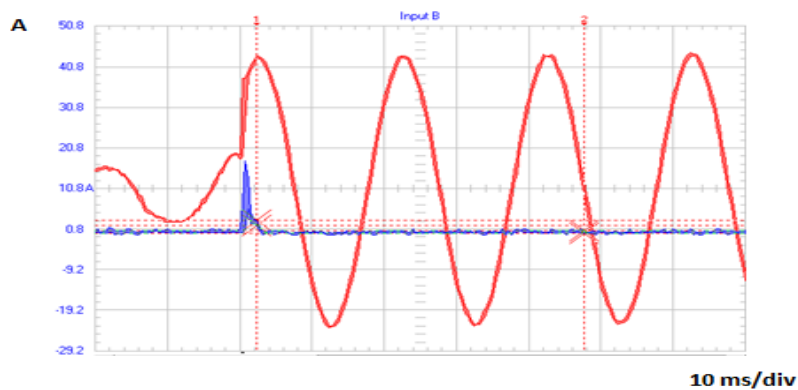


Figure 75: Monitor (power switched in phase 60°)

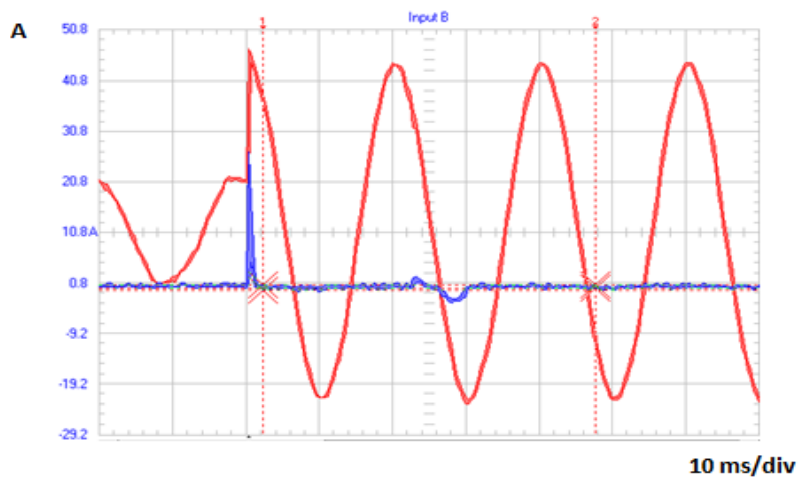


Figure 76: Monitor (power switched in phase 90°)

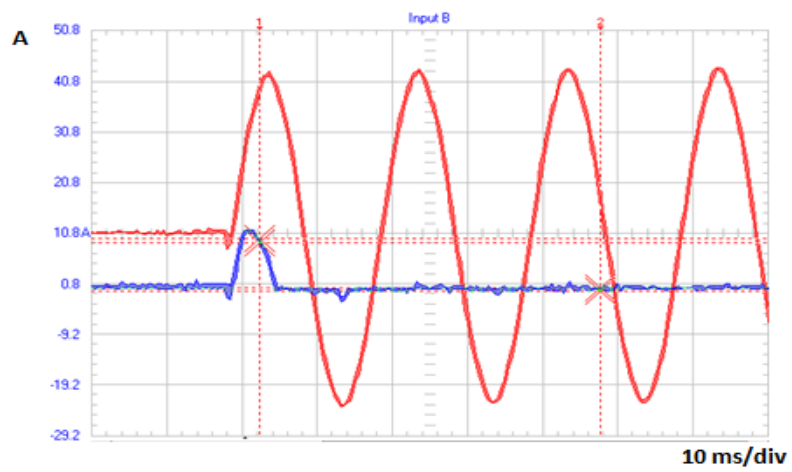


Figure 77: Power Supply (power switched in phase 0°)

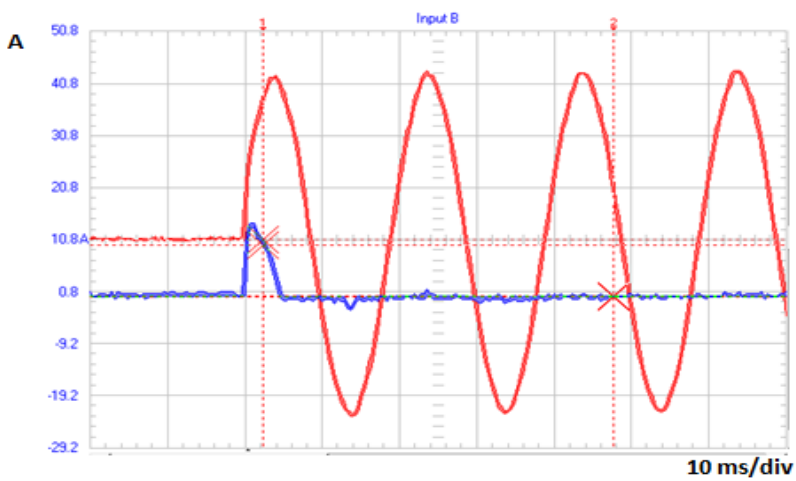


Figure 78: Power Supply (power switched in phase 30°)

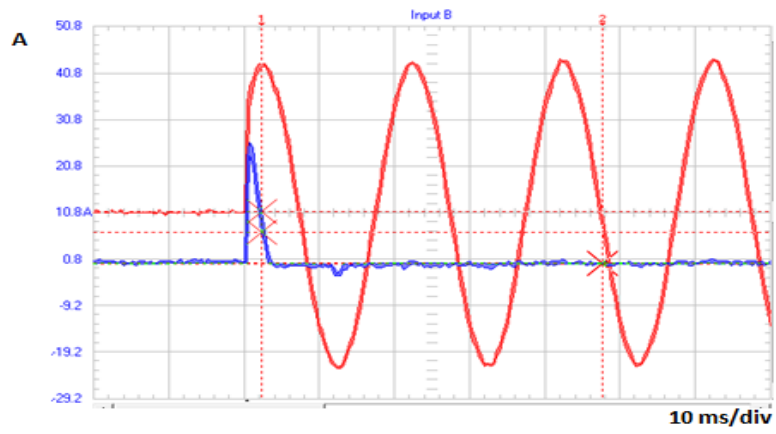


Figure 79: Power Supply (power switched in phase 60°)

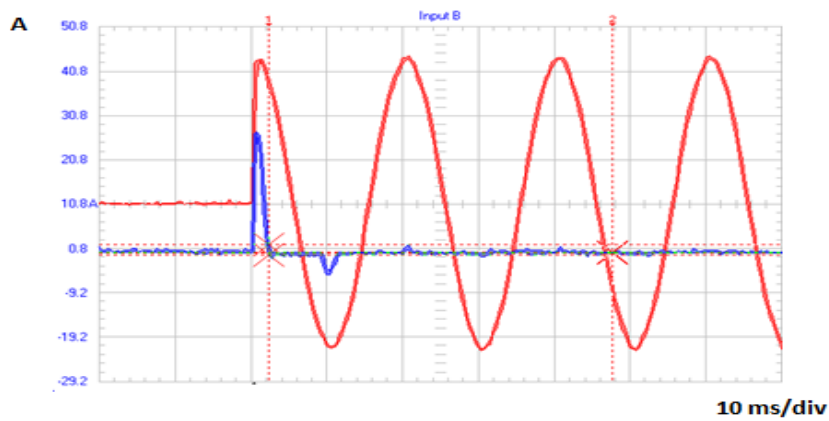


Figure 80: Power Supply (power switched in phase 90°)

To guarantee that the inrush behavior was the same for the correspondent negative phase, extra measurements including the phases -30° , -60° and -90° were done. The correspondent waveforms are present from Figure 81 to Figure 86.

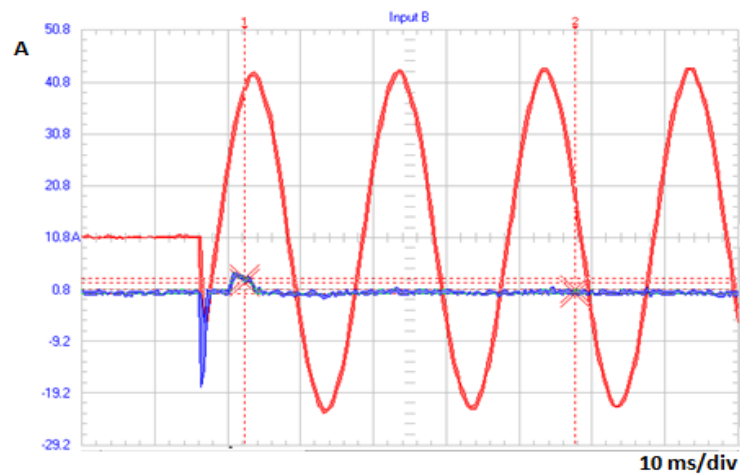


Figure 81: Monitor (power switched in phase -30°)

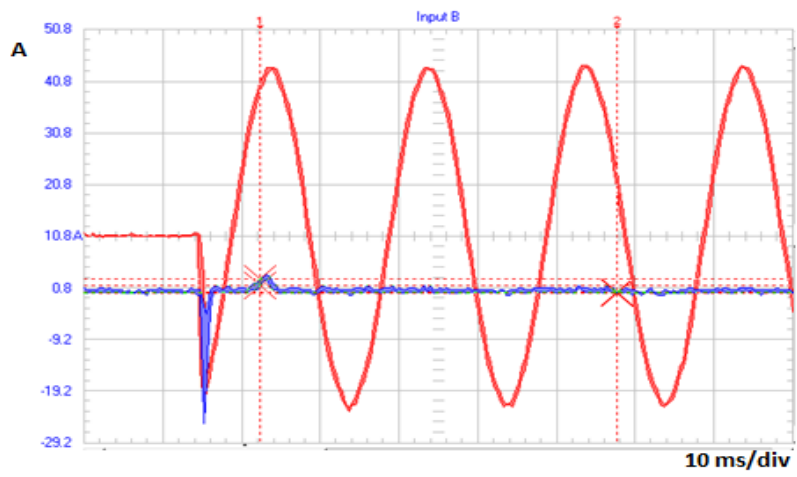


Figure 82: Monitor (power switched in phase -60°)

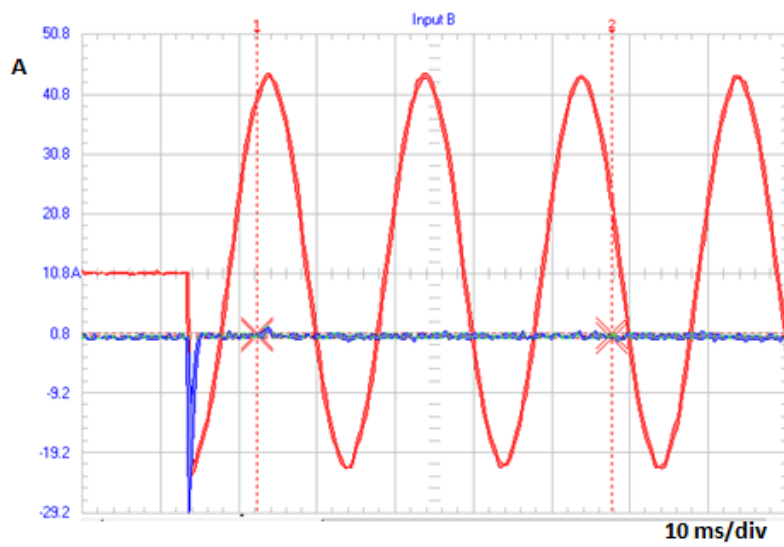


Figure 83: Monitor (power switched in phase -90°)

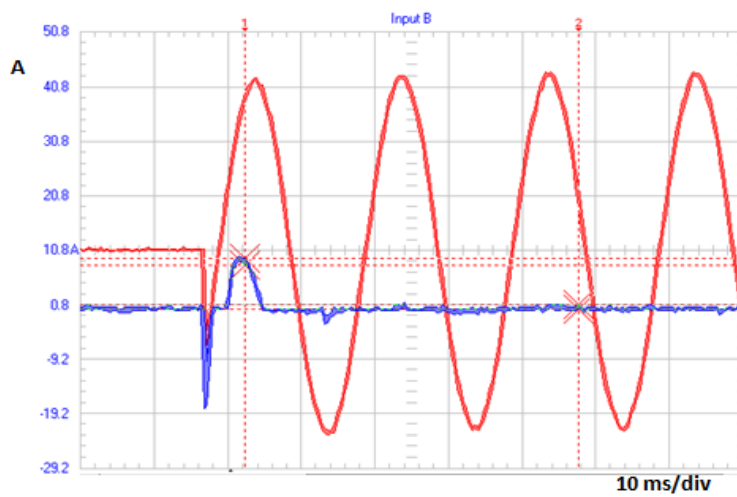


Figure 84: Power Supply (power switched in phase -30°)

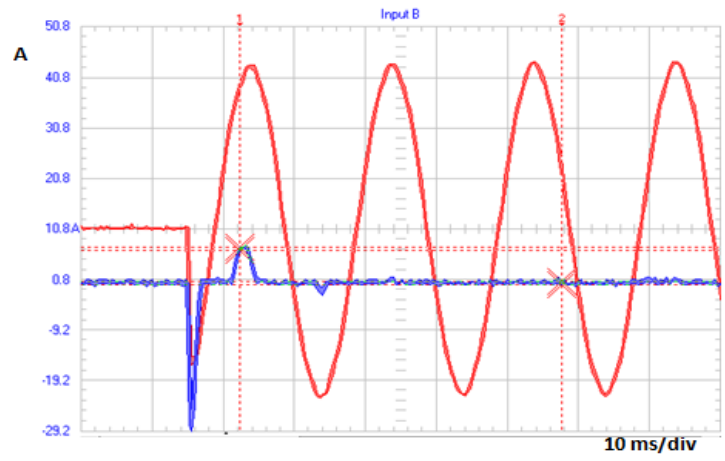


Figure 85: Power Supply (power switched in phase -60°)

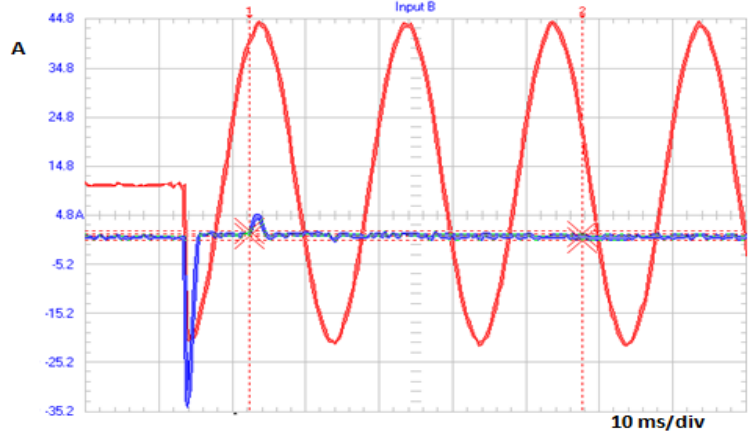


Figure 86: Power Supply (power switched in phase -90°)

The graphs comparing the current waveforms from the models that have been created in LTSpice and the ones measured in the Lab, when the source is switched-on on 0° , 30° , 60° , 90° , -30° , -60° , -90° are present below.

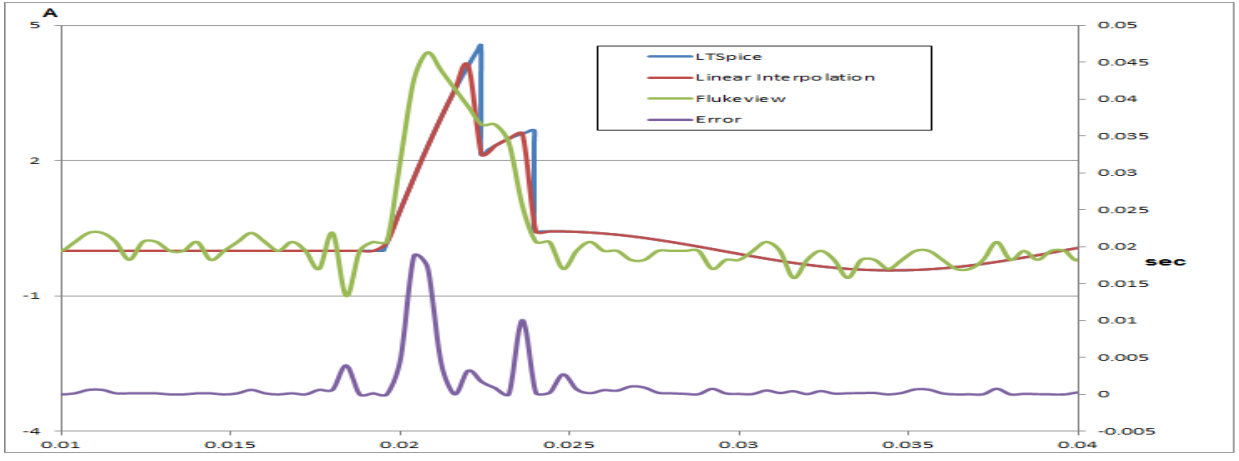


Figure 87: Monitor Phase 0°

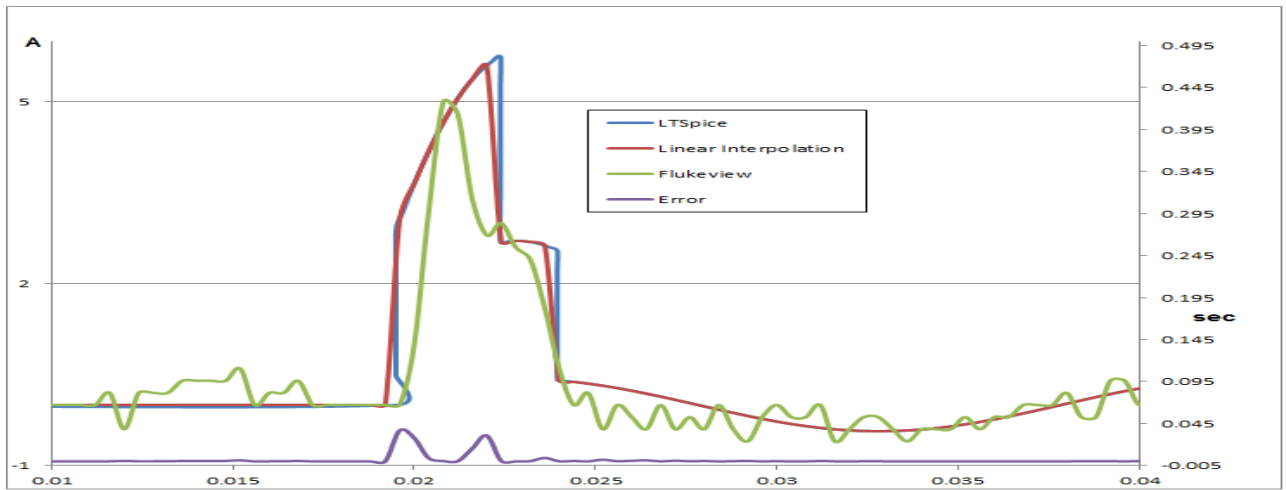


Figure 88: Monitor Phase 30°

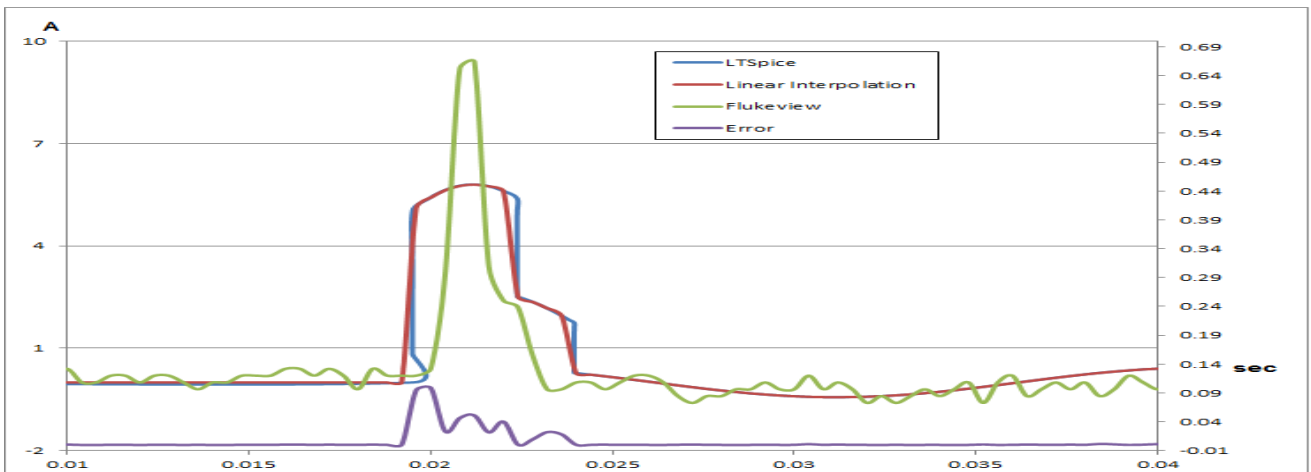


Figure 89: Monitor Phase 60°

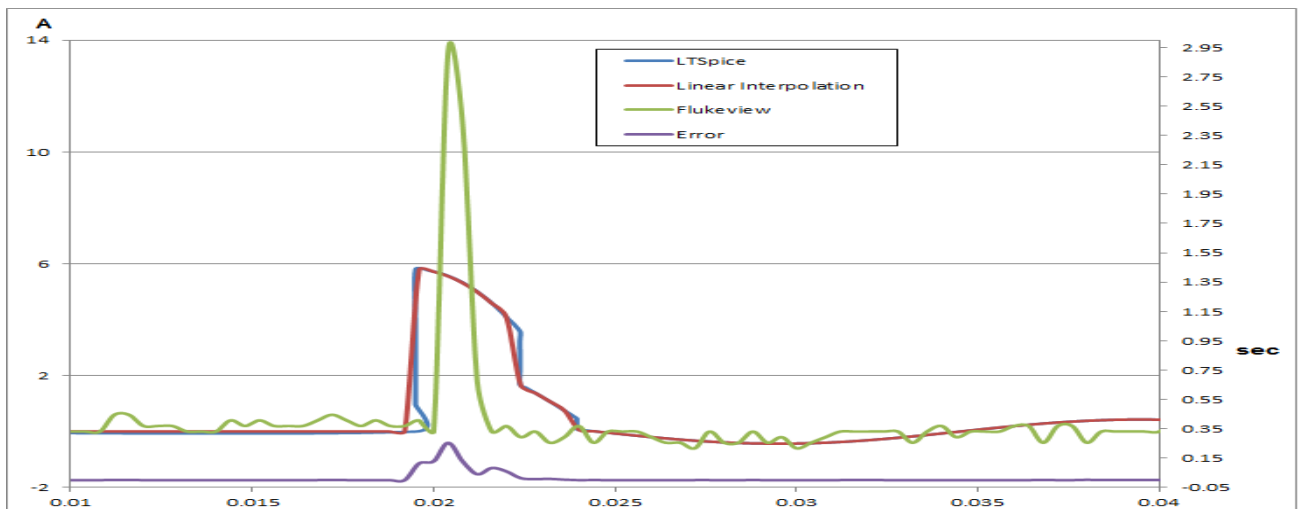


Figure 90: Monitor Phase 90°

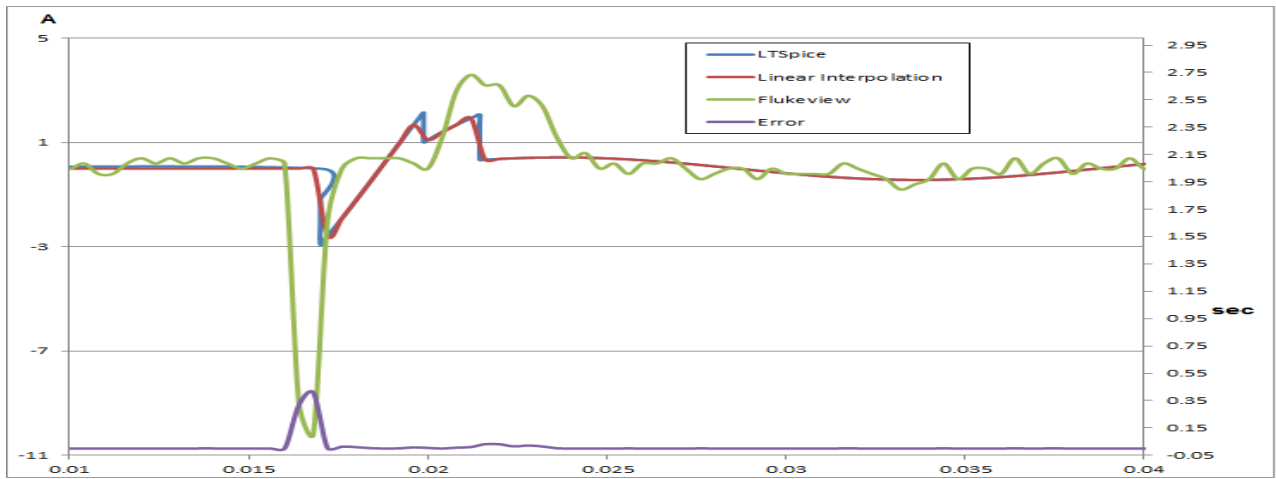


Figure 91: Monitor Phase -30°

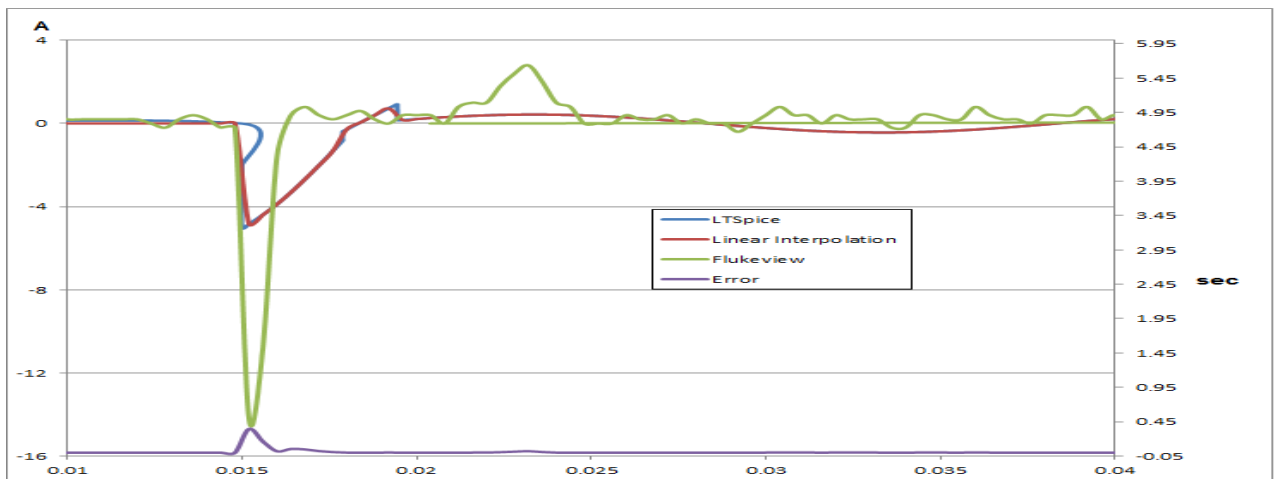


Figure 92: Monitor Phase -60°

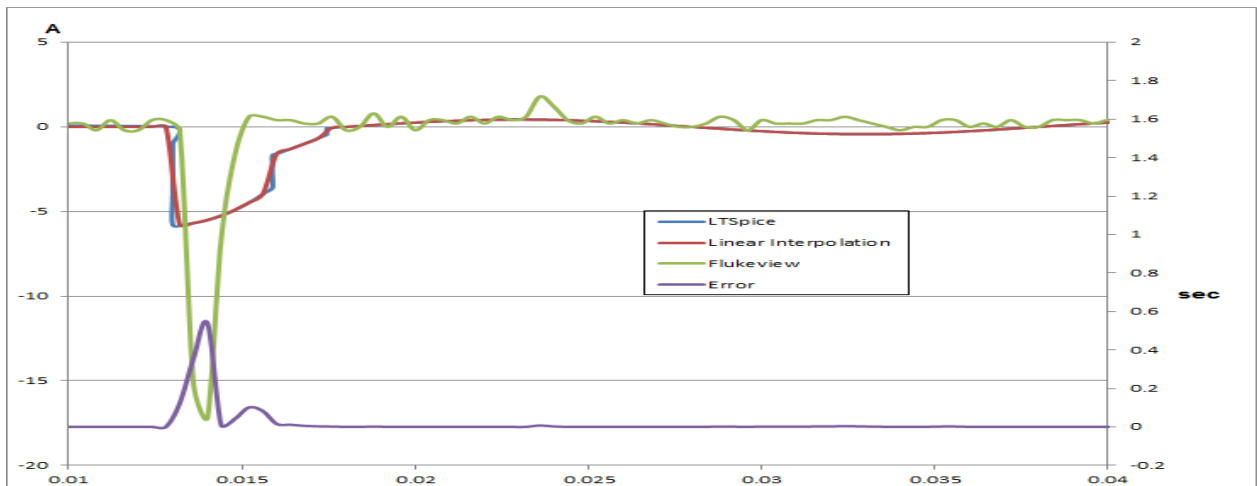


Figure 93: Monitor Phase -90°

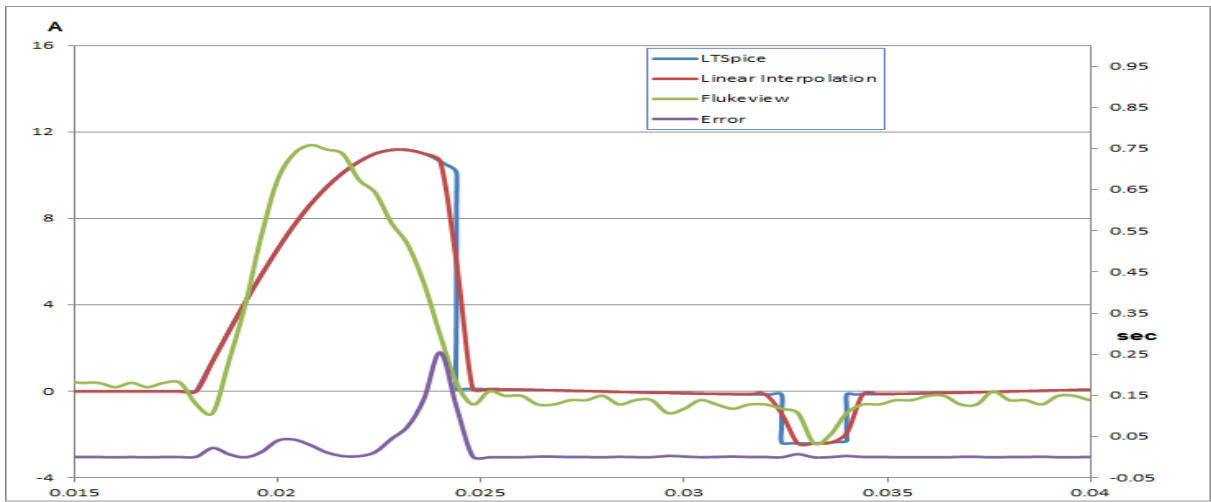


Figure 94: DCPS Phase 0°

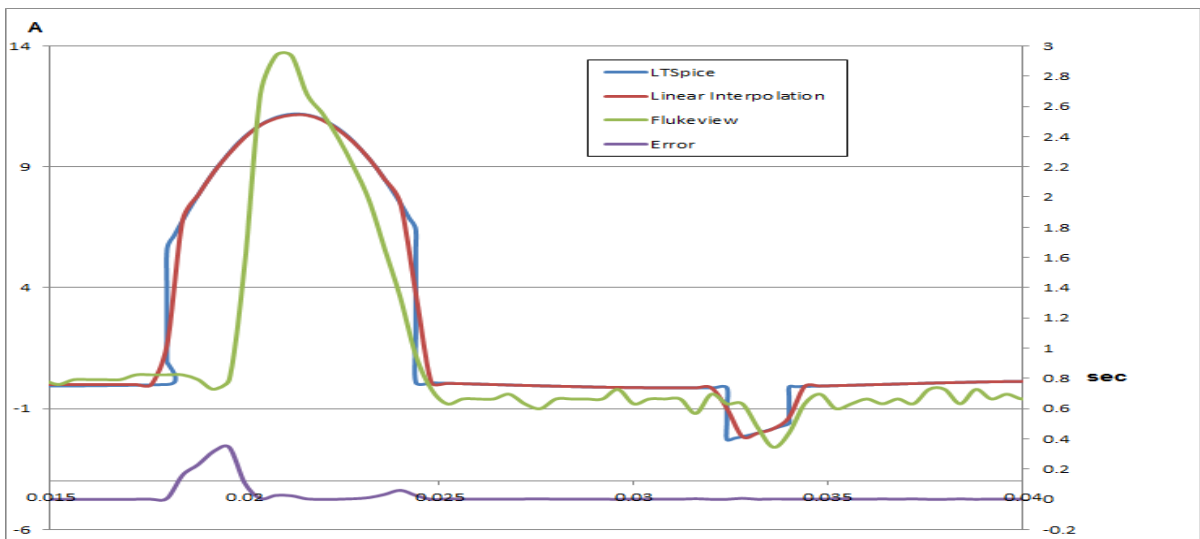


Figure 95: DCPS Phase 30°

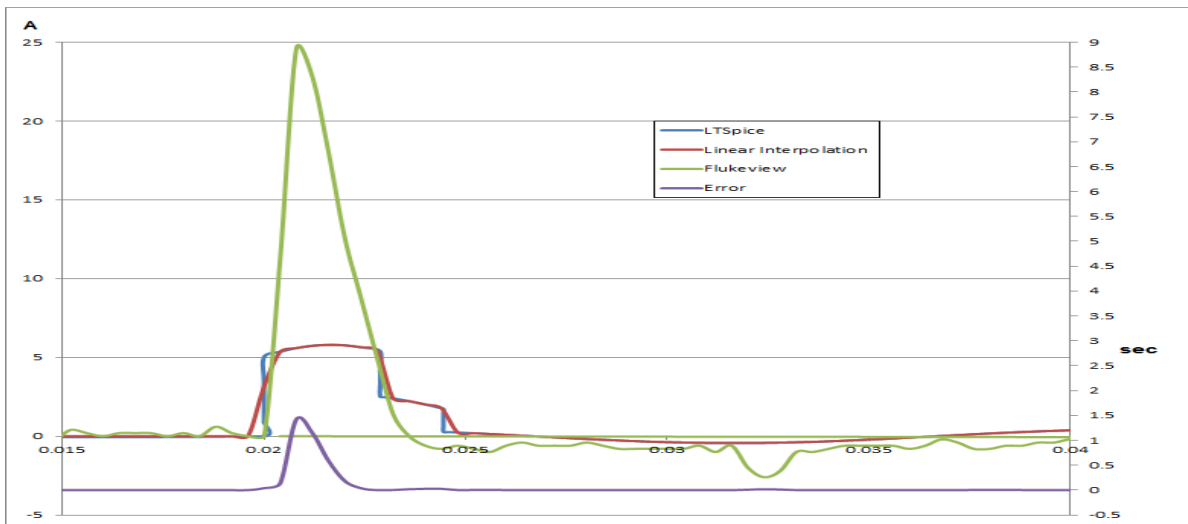


Figure 96: DCPS Phase 60°

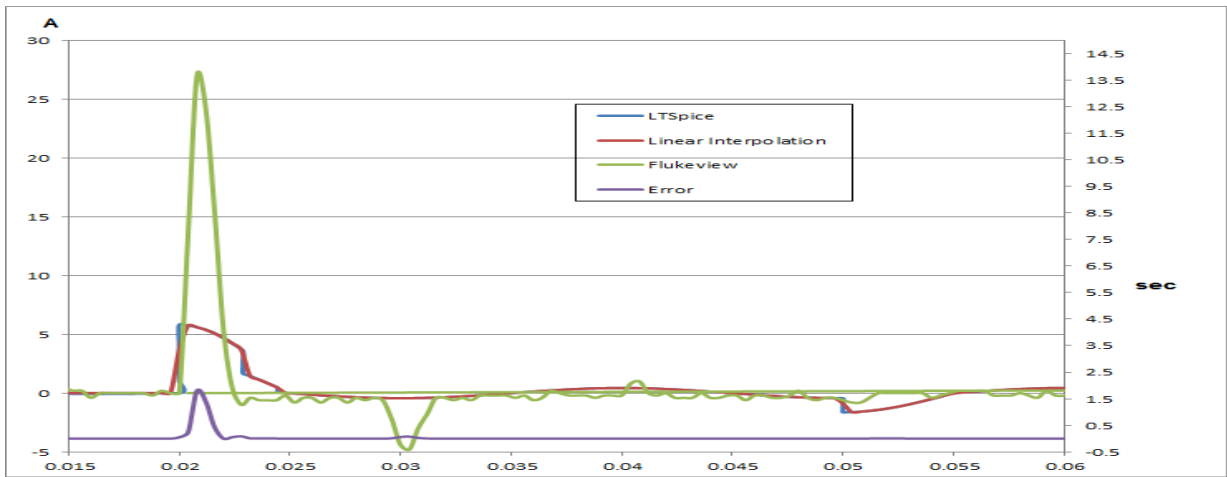


Figure 97: DCPS Phase 90°

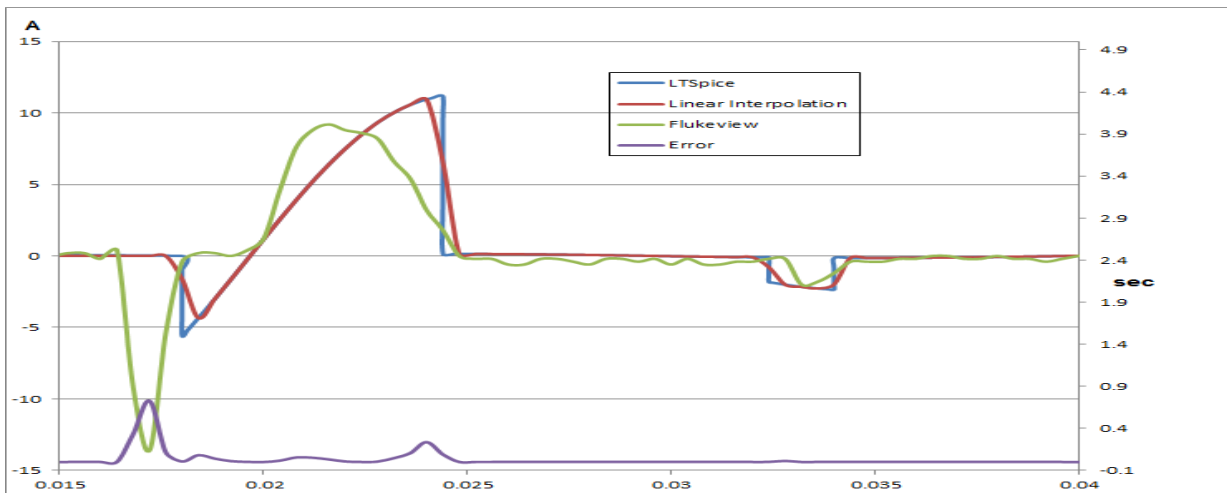


Figure 98: DCPS Phase -30°

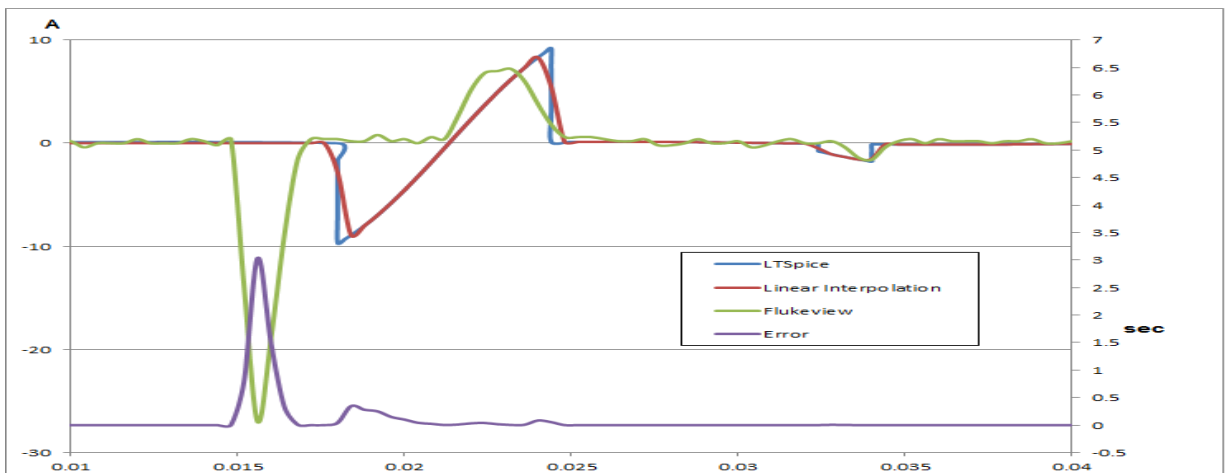


Figure 99: DCPS Phase -60°

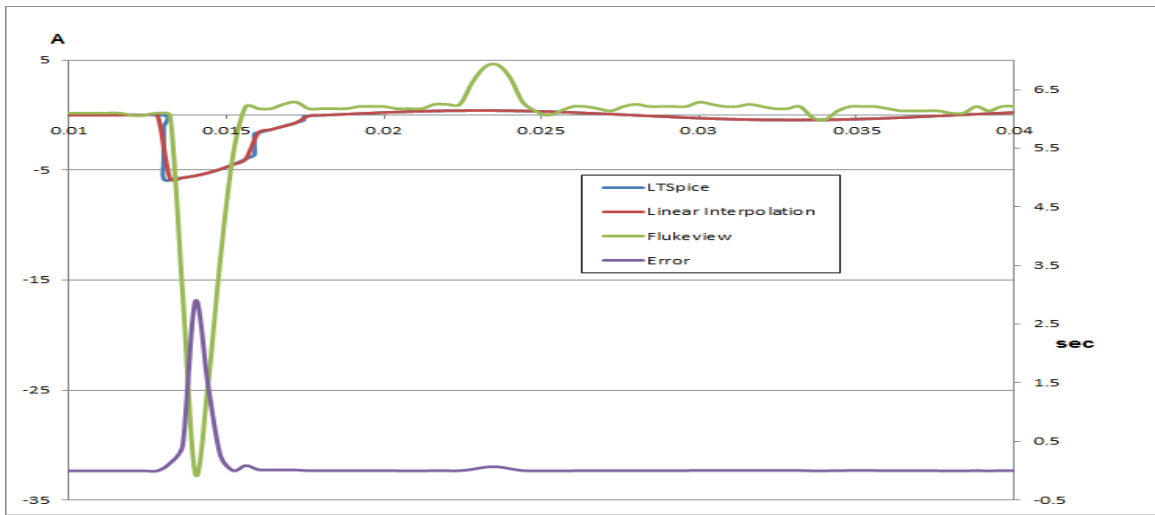


Figure 100: DCPS Phase -90°

REFERENCES

- [1] <http://www.healthcare.philips.com>
- [2] Chen, C. and Wu, Q. 2012. Power Distribution System (PDS) Source and Load Modelling. Philips Healthcare, Best.
- [3] Liu, Y. 2011. Power Distribution System (PDS). Philips Healthcare, Best.
- [4] <http://www.energynetworks.org/info/faqs/electricity-distribution-map.html>
- [5] Boeh-Ocansey, E. and Anizoba, J. 2012. Load Modeling and Behavioral Analysis: Verification and Testing of Power Distribution Unit.
- [6] Sandler, S. Spice Modeling of Magnetic Components. October 7, 2005.
- [7] http://www.math-interactive.com/products/calgraph/help/fit_curve_to_data/root_mean_squared_error.htm
- [8] <http://www.princeton.edu/~achaney/tmve/wiki100k/docs/Varistor.html>